

Contents lists available at ScienceDirect

Petroleum Science

journal homepage: www.keaipublishing.com/en/journals/petroleum-science



Original Paper

A novel fracture-cavity reservoir outcrop geological knowledge base construction method considering parameter collection and processing, mutual transformation of data-knowledge, application and update



Qi-Qiang Ren ^a, Jin-Liang Gao ^{b, *}, Peng Zhu ^c, Meng-Ping Li ^c, Jian-Wei Feng ^d, Qiang Jin ^e, San Zhang ¹

- ^a Institute of Sedimentary Geology, Chengdu University of Technology, Chengdu, 610059, Sichuan, China
- b PetroChina Research Institute of Petroleum Exploration and Development, Beijing, 100083, China
- ^c School of Energy, Chengdu University of Technology, Chengdu, 610059, Sichuan, China
- ^d School of Resources and Geosciences, China University of Mining and Technology, Xuzhou, 221018, Jiangsu, China
- ^e School of Geosciences, China University of Petroleum (East China), Qingdao, 266580, Shandong, China
- f School of Geosciences, Yangtze University, Wuhan, 430100, Hubei, China

ARTICLE INFO

Article history: Received 15 June 2023 Received in revised form 4 December 2023 Accepted 18 February 2024 Available online 20 February 2024

Edited by Jie Hao and Teng Zhu

Keywords: Geological knowledge base Karst fracture-cavity system Mutual transformation of data-knowledge Knowledge base content and application Tarim basin

ABSTRACT

This study endeavors to formulate a comprehensive methodology for establishing a Geological Knowledge Base (GKB) tailored to fracture-cavity reservoir outcrops within the North Tarim Basin. The acquisition of quantitative geological parameters was accomplished through diverse means such as outcrop observations, thin section studies, unmanned aerial vehicle scanning, and high-resolution cameras. Subsequently, a three-dimensional digital outcrop model was generated, and the parameters were standardized. An assessment of traditional geological knowledge was conducted to delineate the knowledge framework, content, and system of the GKB. The basic parameter knowledge was extracted using multiscale fine characterization techniques, including core statistics, field observations, and microscopic thin section analysis. Key mechanism knowledge was identified by integrating trace elements from filling, isotope geochemical tests, and water-rock simulation experiments. Significant representational knowledge was then extracted by employing various methods such as multiple linear regression, neural network technology, and discriminant classification. Subsequently, an analogy study was performed on the karst fracture-cavity system (KFCS) in both outcrop and underground reservoir settings. The results underscored several key findings: (1) Utilization of a diverse range of techniques, including outcrop observations, core statistics, unmanned aerial vehicle scanning, high-resolution cameras, thin section analysis, and electron scanning imaging, enabled the acquisition and standardization of data. This facilitated effective management and integration of geological parameter data from multiple sources and scales. (2) The GKB for fracture-cavity reservoir outcrops, encompassing basic parameter knowledge, key mechanism knowledge, and significant representational knowledge, provides robust data support and systematic geological insights for the intricate and in-depth examination of the genetic mechanisms of fracture-cavity reservoirs. (3) The developmental characteristics of fracturecavities in karst outcrops offer effective, efficient, and accurate guidance for fracture-cavity research in underground karst reservoirs. The outlined construction method of the outcrop geological knowledge base is applicable to various fracture-cavity reservoirs in different layers and regions worldwide. © 2024 The Authors. Publishing services by Elsevier B.V. on behalf of KeAi Communications Co. Ltd. This

is an open access article under the CC BY license (http://creativecommons.org/licenses/by/4.0/).

1. Introduction

The Ordovician carbonate strata in the Tarim Basin boast a rich karst fracture-cavity system (KFCS), a resourceful repository of oil

Corresponding author. E-mail address: jinliang0205@126.com (J.-L. Gao).

and gas (Tian et al., 2016; Zhang et al., 2018; Chen et al., 2021; Zeng et al., 2022). Governed by concurrent tectonic activity and karst fluid processes, the KFCS embodies a fault-fracture-cavity system genetically linked to distinct fracture-cavity units (Loucks, 1999; Rongier et al., 2014; Xie et al., 2021; Méndez et al., 2021). The diverse tectonic activities and fluid types have led to the identification of superimposed development characteristics in various KFCS units (Firme et al., 2021; Li et al., 2022), Consequently, a range of dissolution and filling combinations, intricate spatial configurations, and distribution patterns has emerged (Mazzullo, 2004; Wang et al., 2019; Ren et al., 2020a; Fu et al., 2023). Analyzing the differences in composition and combination within the KFCS offers valuable insights into structural and fluid details, playing a crucial role in comprehending the developmental characteristics and formation mechanisms. Trace element geochemical testing enables an effective differentiation between KFCS fillings and wall rock, allowing for a detailed description of the internal composition structure of the fillings and preliminary identification of fluid type and source (Cai et al., 2020; Araújo et al., 2021; Zeng et al., 2023). Understanding the patterns of filling combinations and fracturecavity associations holds significant importance in unraveling the developmental characteristics and genetic mechanisms of the KFCS (Zhong et al., 2021; Bagni et al., 2022).

Guided by the coupled dissolution-filling mechanism arising from multi-field interactions involving structural, fluid, chemical, and thermal factors, the fracture-cavity system exhibits pronounced heterogeneity (Castillo and Mann, 2006; Haeri et al., 2013; Ren et al., 2020a). Fracture-cavities and their fillings are widely distributed, forming in diverse settings such as the runoff zone (underground river), fault-controlled cavities, and epikarst regions (Zhong et al., 2012; Méndez et al., 2020; Ren et al., 2021; Zhang et al., 2021). Comprehending the dissolution and filling development patterns across different tectonic environments, fluid types, and temperature fields is crucial for unraveling the formation and evolution mechanism of the KFCS (Castillo and Mann, 2006; Zhong et al., 2012; Amirjan and Bozorg, 2018; Mao et al., 2018; Yadav et al., 2021). Throughout the formation period of the KFCS, tectonic activities such as faulting, fracturing, and folding impact the normal dissolution rate of carbonate rocks, resulting in changes in dissolution direction and filling location (Ren et al., 2020a; Cavailhes et al., 2022; Ning et al., 2022). Additionally, the dissolution and filling mechanism of the KFCS can be influenced by changes in meso-small fractures and effective tectonic stress, giving rise to distinctive spatial combination patterns (Ren et al., 2020a; Xiong et al., 2021; Negahdari et al., 2022).

The fragmented state of knowledge regarding the formation and evolution of the KFCS has resulted in scattered insights, primarily due to the absence of effective management methods (Ma et al., 2022; González-Esvertit et al., 2022). Achieving a comprehensive understanding of geological knowledge has proven exceedingly challenging, fostering one-sided and fragmented research on karst reservoirs and impeding the capacity for complex and in-depth studies (Hassanzadeh et al., 2022; González-Esvertit et al., 2023). For the construction of the reservoir outcrop GKB, three pivotal components were identified: knowledge definition, extraction, and application, with knowledge extraction emerging as the most intricate and critical challenge (He et al., 2021; Ren et al., 2020b). Integrating various geological data from clastic rock reservoirs through training images facilitates the acquisition of information on sedimentary genesis, scale, spatial morphology, and distribution patterns (Castillo and Mann, 2006). The exploration of underground reservoirs can be effectively guided by the achievements and knowledge garnered from outcrop studies, overcoming challenges related to poor continuity, large-scale differences, and data limitations (Jin et al., 2017; He et al., 2021; Lyu et al., 2021).

However, conducting more complex and in-depth research on the genetic mechanism remains a challenge (Ren et al., 2020b; He et al., 2021). Presently, there exists no clear definition for GKB construction and knowledge extraction. The coupling of KFCS study with artificial intelligence still poses an urgent scientific problem that needs to be addressed.

In this manuscript, our primary objective is to offer a comprehensive insight into the construction of the reservoir outcrop GKB for the KFCS. We conducted a thorough assessment of traditional geological achievements and knowledge to define the geological knowledge framework, content, and system. The basic parameter knowledge of the KFCS was meticulously extracted through multiscale fine characterization methods, encompassing core, outcrop, and thin section observations. Key mechanism knowledge was derived from the analysis of filling trace elements, isotope geochemical tests, and water-rock simulation experiments. Additionally, we employed a combination of multiple linear regression, neural network technology, discriminant classification, and expert judgment techniques, utilizing SPSS Statistics 17.0 software, to unearth significant representational knowledge. Concluding our methodology, we conducted an analogy study on the developmental characteristics of the KFCS, drawing comparisons between outcrops and underground reservoirs. This provided a systematic understanding of the complex and in-depth study on the genetic mechanism of fracture-cavity reservoirs. The developmental characteristics of the KFCS in outcrops offer effective, efficient, and accurate guidance for fracture-cavity research in underground karst reservoirs. Importantly, the construction method of the outcrop geological knowledge base can be universally applied to various fracture-cavity reservoirs in diverse layers and regions worldwide.

2. Geological setting

The study area is situated in the northern Tarim Basin in China, encompassing both typical karst outcrops and the Tahe oilfield (Fig. 1a) (Li and Gao, 2014). Structurally, the typical karst outcrops are positioned near the Keping and Bachu fault uplifts, while the Tahe oilfield is situated between the Kuqa depression and North Tarim uplift (Fig. 1b) (Tian et al., 2016). The karst region is categorized into three types: the runoff zone, fault-controlled cavities, and epi-surface cavities, illustrated by the Yijianfang, Liuhuanggou, and Xekar profiles, respectively (Li and Gao, 2014; Shi et al., 2014). The Yijianfang profile spans over 50 km along Province way 218 (11 km) in Xinjiang Province, China, extending from Keping city to Tumushuke city. The Liuhuanggou profile is situated along National way 314 (1135 km) in Bachu County, China. The Xekar profile is developed along National way 314, approximately 8 km from Xekar town (Fig. 1c) (Zhong et al., 2012; Ren et al., 2020b). The Tahe oilfield is positioned at the Akkule bulge, an ancient tectonic structure (Fig. 1d), where deformation has been significantly influenced by multiple tectonic orogenies, including the Caledonian and Hercynian events (Tian et al., 2016).

During the Caledonian-Hercynian orogenies, the study area underwent intense and intricate karstification processes, leading to the development of diverse fracture-cavity categories and stages associated with meteoric water, formation karst water, and hydrothermal fluids (He et al., 2010; Chen et al., 2012; Ren et al., 2021). Three significant hydrothermal events have been identified in the study area: the Late Caledonian-Early Hercynian, Late Hercynian, and Himalayan events (Jin et al., 2013; Lu et al., 2015). Throughout the deposition periods, the dissolution process by meteoric waters was influenced by tectonic uplift and angular unconformities at the end of the Devonian and Permian periods. The studied rocks belong to the Penglaiba, Yingshan, Yijianfang, and Dawangou groups, representing Ordovician fracture-cavity

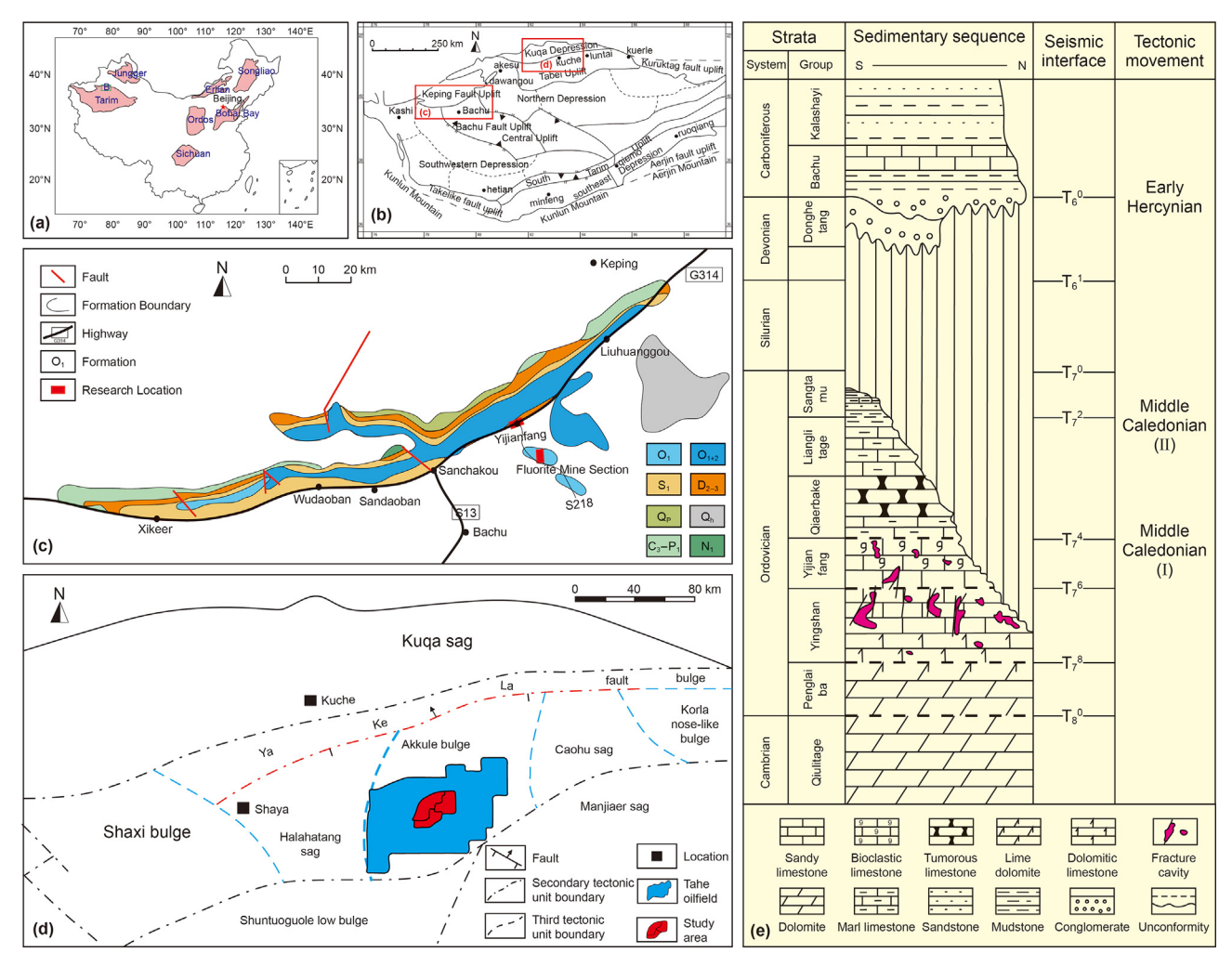


Fig. 1. Regional tectonic location of the study area. (a) refers to the location of Tarim Basin in China; (b) shows the tectonic characteristics of Keping and Bachu area; (c) represents the location of the Tahe oilfield; (d) is stratigraphic histogram of the Paleozoic; (e) refers to the strata characteristics in the study area.

carbonate formations comprising bioclastic limestone, lime dolomite, and dolomitic limestone (Fig. 1e) (Zhong et al., 2012; Li and Gao, 2014). The karstic formation in the research area has a total thickness of up to 600 m. Specifically, the Yingshan formation, influenced by the KFCS, has an approximate thickness of 250 m, with its extension direction following the strike of the main faults (Chen et al., 2012; Méndez et al., 2020). The fillings within the KFCS can be categorized into chemical minerals and mechanical sediments, encompassing calcite, sulfur, gypsum, fluorite, collapsed breccia, exfoliating conglomerate, and sandstones (Tian et al., 2016).

3. Techniques and methods

3.1. Technologies of knowledge definition, extraction, and application

The structural analysis method and Analytic Hierarchy Process (AHP) were applied to elucidate the strengths and weaknesses inherent in traditional geological knowledge. In considering the formation and generation mechanism of the KFCS, diverse geological knowledge relevant to fracture-cavity reservoir research was seamlessly integrated, resulting in the establishment of a

comprehensive knowledge system for KFCS. Building upon prior investigations into spatial combination characteristics and genetic evolution mechanisms, fundamental geological parameters, genetic evolution mechanisms, and key geological characterization elements closely associated with KFCS were clarified. By accounting for the mutual coupling relationship between different geological parameters, the knowledge framework and content for KFCS were precisely defined. This systematic process revealed the definition and composition of basic parameter knowledge, key mechanism knowledge, and significant representational knowledge for KFCS (Fig. 2). Concretely, basic geological parameter knowledge was defined as parameters suitable for characterizing the morphological distribution of different fracture-cavity categories. Key mechanism knowledge encompassed internal mechanisms and formation results (such as formation period, environment, and fluid source, etc.) accessible through geochemical testing and detailed analysis. Significant representational knowledge was defined as crucial geological parameters applicable to distinguishing various fracture-cavity types through various mathematical analysis methods. Consequently, an analogy study on the developmental characteristics of fracture-cavities between outcrops and underground reservoirs was undertaken utilizing the obtained knowledge system.

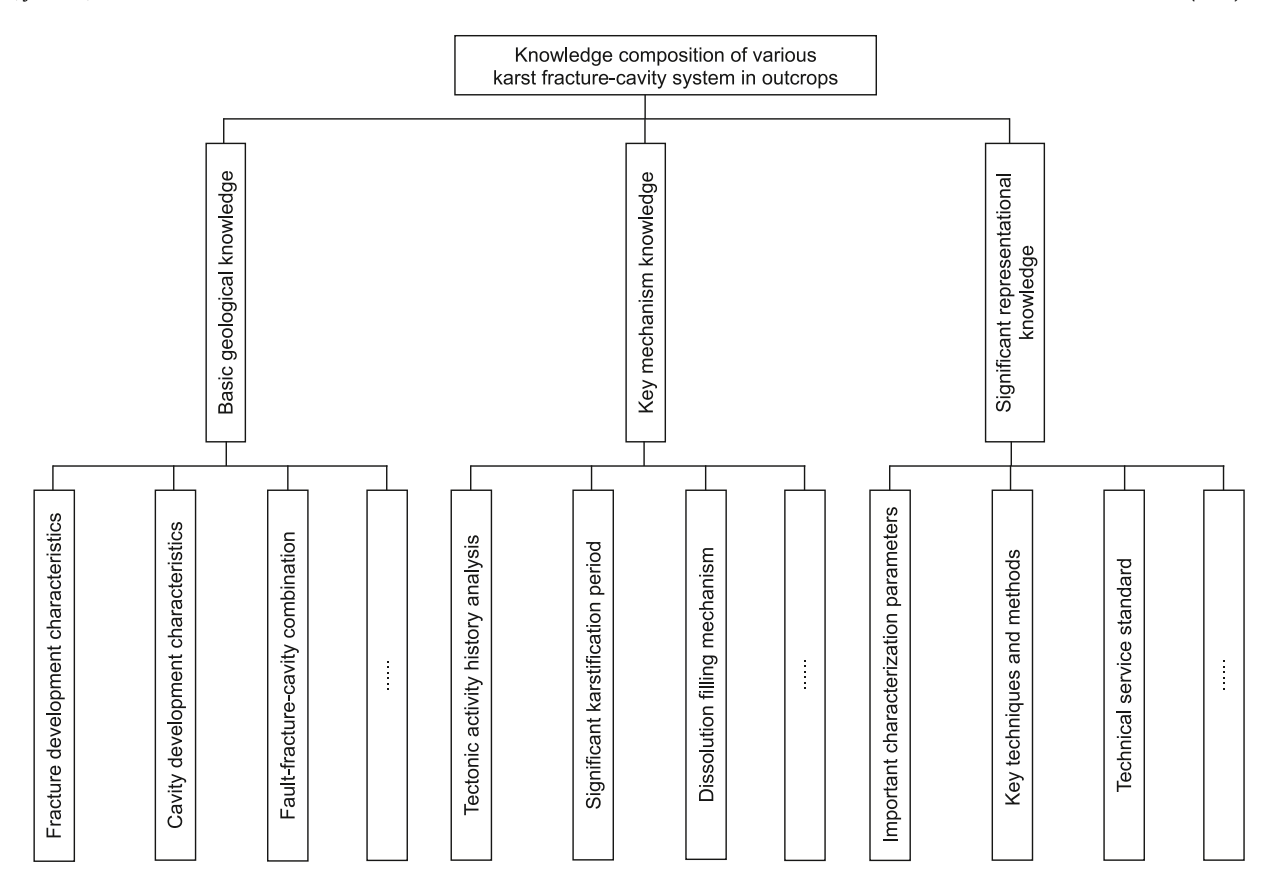


Fig. 2. The schematic diagram of knowledge framework system for fracture-cavity outcrop reservoir.

3.2. Multiple scale fine characterization techniques

Field observations, drilling core statistics, and quantitative measurement methods were employed to investigate the macro characteristics of fracture-cavities. Various geological parameters, including faults, fractures, cavities, fillings, and wall rocks, were systematically collected using tools such as cameras, tapes, compasses, geological hammers, GPS devices, and ropes. Additionally, unmanned aerial vehicles and laser scanners were utilized to enhance data collection efficiency. Through meticulously exploration and measurement, the basic geological parameters characterizing the morphological distribution of different fracture-cavity categories were systematically summarized. Then samples of cavity fillings, fracture fillings, and wall rocks were collected for element geochemical testing. For the study of micro fracture-cavity characteristics, cast thin section observations and electron scanning experiments were conducted. Cast thin sections were employed to delineate the intricate combination patterns among fractures, cavities, dissolution features, and fillings at a micro scale. The thin sections of specimens were prepared using a ZT-2 high-pressure casting machine at the Petroleum Geology Testing Center of China Petroleum and Chemical Corporation (CPCC). Electron scanning experiments were conducted using a Quanta 200 scanning electron microscope and EDAX spectrometer online equipment at the petroleum geology testing center, facilitating the analysis of chemical compositions in wall rocks, fracture fillings, and cavity fillings. Through both macro and micro observations, the developmental characteristics of diverse fracture-cavity categories were described in meticulous detail.

3.3. Isotope-trace element testing and water-rock interaction numerical simulation

To examine the fluid source, composition, and precipitation mechanism within the KFCS, this study utilized carbon and oxygen isotopes, along with strontium isotopes. The analysis of key mechanism knowledge was intricately linked with numerical simulations of water-rock interactions. Carbon and oxygen isotopes underwent testing using a gas isotope mass spectrometer (MAT 253) at the Petroleum Geology Testing Center, CPCC, following the method outlined in "Determination of carbon and oxygen isotopes in carbonate minerals or rocks" (Jia et al., 2017). The stability of ¹³C and ¹⁸O isotopes served to elucidate the source and formation environment of the KFCS (Shi et al., 2014). The strontium isotope experiment was conducted at the Analysis and Testing Center of the Beijing Institute of Geology, Nuclear Industry, utilizing a Phoenix hot surface ionization mass spectrometer, boasting a maximum accuracy of 3%, a temperature of 20 °C, and a humidity of 40%. Determination of the paleo sedimentary environment of the KFCS was based on the value of ⁸⁷Sr/⁸⁶Sr, following the protocol outlined in "Determination of Lead, Antimony, and Strontium Ions in Rocks." Trace elements were examined using a plasma mass spectrometer (NexION300D, No.10742) at the Analysis and Testing Center of the Beijing Institute of Geology, Nuclear Industry, adhering to the standard "Carbonate rock chemical analysis method: Determination of 44 elements." The testing temperature and relative humidity were set at 22 °C and 21%, respectively.

Building upon the results of geochemical testing, an analysis was conducted on the fluid type, composition, and precipitation

mechanism. Subsequently, the Water-Rock Interaction Simulation (WRIS) software (PetraSim, 2016) was employed to delve into the dissolution and filling processes within the KFCS. In this endeavor, the WRIS utilized two primary modules, Tough-2 and Tough-react. The Tough-react module, integral to the WRIS, incorporates reactions between mineral aggregates and liquids under local equilibrium or dynamic rate conditions, specifically focusing on nonisothermal flow chemical reactions in multiphase fluids. Two key systems, namely anhydrous $CaCl_2-(NH_4)_2CO_3-NH_4Cl$ and the thermodynamic $CO_2-H_2O-CaCO_3-NaCl$ system, were deployed to simulate the precipitation and dissolution processes. The chemical reactions involved in the numerical simulation were classified into two significant groups.

① With a small amount of CO₂ injection:

 $CaCl_2+(NH_4)_2CO_3$ = $CaCO_3$ (precipitation) + NH_4Cl , And $CO_2+Ca(OH)_2$ = $CaCO_3$ (precipitation) + H_2O .

② With a large amount of CO₂ injection:

 $CO_2+H_2O+CaCO_3+2NaCl=2NaHCO_3+CaCl_2$ (dissolution). During the injection process, the dissolution and filling generally formed simultaneously.

3.4. Data processing and characterization techniques

To unveil the significant representational knowledge of the KFCS, this manuscript employed multivariate linear regression. neural network techniques, and discriminant classification. Multivariate linear regression, a method establishing mathematical relationships between dependent variables and two or more variables, extended the univariate model (Abba et al., 2017; Wang et al., 2020; Bozorgmanesh et al., 2020). It was utilized to analyze the correlations among fracture-cavity categories and various geological parameters. The neural network technique was employed to differentiate the fracture-cavity categories, encompassing three key steps: data preparation, formula fitting, and predictive analysis. During data preparation, collected geological parameters were matched with the corresponding fracture-cavity categories. Based on the determined fracture-cavity category, an intrinsic characterization formula was established. This formula was then used to predict unknown fracture-cavity categories, and the accuracy of the predictions was verified. Finally, the discriminant classification method was employed to conduct a detailed analysis of the fracture-cavity categories. The database was utilized, allocating 80% and 20% of the data for testing and validation, respectively. Quantitative characterization formulas were derived to establish relationships between fracture-cavity categories and geological parameters. Through the integration of multivariate linear regression, neural network techniques, and discriminant classification, the significant geological parameters for characterizing fracture-cavity reservoirs were determined.

4. Results

4.1. Establishment of geological knowledge framework of karst reservoir outcrop

To refine the characterization of the KFCS, four key aspects were chosen for detailed examination: fracture-cavity geometry, fault-fracture characteristics, fracture-cavity filling, and combination features (Fig. 3). The research structure was defined across three levels: data collection, mutual transformation of data and knowledge, and knowledge application. Additionally, the KFCS

knowledge system embraced three essential components: basic parameter knowledge, key mechanism knowledge, and significant representational knowledge.

In the data collection phase, comprehensive knowledge about the basic parameters of the KFCS was gathered using advanced fine characterization techniques at multiple scales. This encompassed details such as cavity width, height, depth, 3D data, associated fault fractures, fault extension strike, morphological characteristics, fracture length, orientation, density, fracture filling features, cavity filling features, wall rock features, filling distribution law, filling combination characteristics, fracture-cavity combination, fault-fracture combination, and fault-fracture-dissolution-filling combination features. Particularly meticulous descriptions were provided for fracture and cavity parameters, along with combinational patterns aimed at elucidating distinct karst categories.

The crucial step of mutual transformation of data and knowledge, integral to the construction of the GKB, was accomplished through geological analysis, geochemical testing, numerical simulation, and mathematical processing. Building upon the collected basic parameter knowledge, key mechanism knowledge was derived using geostatistics, the analytic hierarchy process (AHP), geochemical analysis, and water-rock simulation. Two vital components of key mechanism knowledge were identified: the fluid source, composition, precipitation mechanism, and evolutionary process of dissolution and filling characteristics. Employing methods such as multivariate linear regression, neural network techniques, discriminant classification, and expert judgment systems, significant geological parameters characterizing diverse fracture-cavity categories were discerned. Consequently, significant representational knowledge of the KFCS was incorporated into the geological knowledge base. Through the integration of basic parameter knowledge, key mechanism knowledge, and significant representational knowledge of the KFCS, an analogical study of the development characteristics of fracture-cavity systems between typical outcrops and underground karst reservoirs was conducted.

4.2. The basic parameter knowledge of KFCS in different categories

The primary stream cavity, sculpted along pre-existing faults or large-scale fractures, displayed a continuous pipe-like structure featuring minimal collapsed filling, multi-stage underground river deposits, and high-angle conjugate fractures (Fig. 4a and e). The tributary cavity, influenced by meso-scale and small-scale fractures, exhibited a comparatively smaller scale (Fig. 4b and f). The hall cavity, influenced by small faults, was characterized by expansive vertical and horizontal pipelines, along with diverse types of internal fillings (Fig. 4c and g). Additionally, the terminal cavity, affected by small-scale fractures, interconnected with the surrounding strata of the primary stream cavity or the tributary cavity, encompassing sedimentary debris and chemical fillings (Fig. 4d and h).

The primary stream cavity exhibited a diverse range of morphologies, encompassing nearly circular, nearly elliptical, and square-like shapes (Fig. 5). Cavity dimensions were distributed within the ranges of 0.50–4.95 m for height, 0.45–6.95 m for width, and 5.39–17.90 m for depth. Additionally, the aspect ratio of width to height varied from 1.15 to 3.09, while the aspect ratio of depth to height fell within the range of 0.84–7.15. The pre-karstification, during karstification, and post-karstification fracture densities ranged from 0.45 to 0.73, 0.31 to 0.61, and 0.83 to 1.66 fractures/m, respectively. The tributary cavity displayed morphologies ranging from nearly elliptical to elongated strip-like shapes. The cavity dimensions were in the ranges of 0.23–3.50 m for height, 0.40–6.04 m for width, and 0.57–9.93 m for depth. The width/height ratio varied from 1.15 to 5.7, and the depth/height

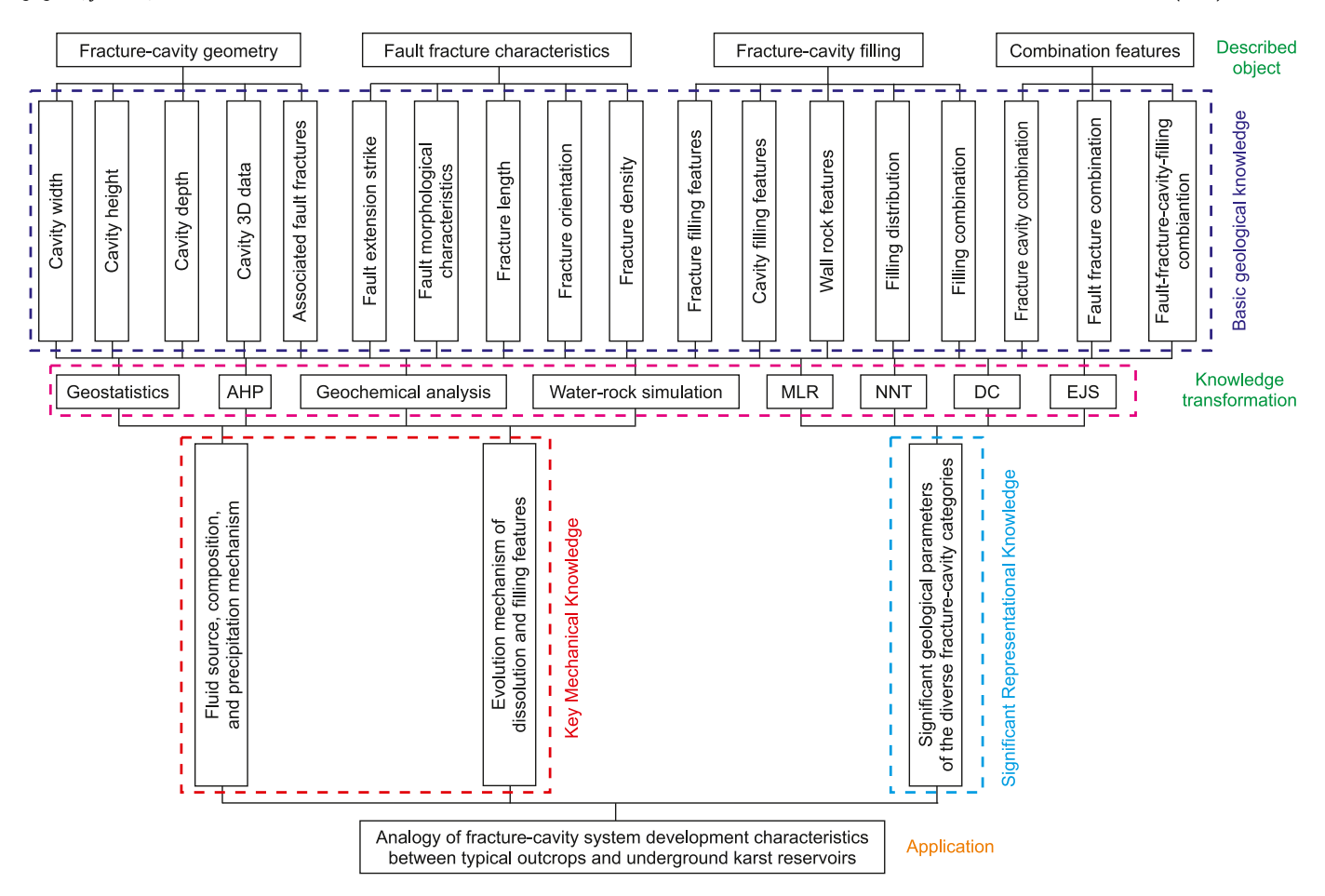


Fig. 3. The knowledge framework system of karst reservoir outcrop (underground river) (AHP is analytic hierarchy process, MLR refers to multivariate linear regression, NNT is neural network technique, DC represents the discriminant classification, EJS is expert judgement system).

ratio ranged from 0.62 to 6.63. The fracture density during the periods before karstification, during karstification, and after karstification followed a similar pattern, ranging from 0.45 to 0.73, 0.31 to 0.61, and 0.83 to 1.66 fractures/m, respectively.

In the hall cavity, the height, width, and depth were within the ranges of 8.59–13.37 m, 15.30–21.40 m, and greater than 4.00 m, respectively. The width/height and depth/height ratios were both greater than 1, ranging from 0.29 to 0.46. Fracture density during the periods before, during, and after karstification ranged from 0.50 to 1.75, 0.5 to 1, and 0.50 to 1.25 fractures/m, respectively. For the tip cavity, height, width, and depth ranged from 0.50 to 1.96 m, 0.60–3.64 m, and 0.80–7.34 m, respectively. The width/height and depth/height ratios were in the ranges of 1.20–1.86 and 1.60–5.79, respectively. Fracture density during the periods before, during, and after karstification ranged from 0.10 to 0.30, 0.10 to 0.20, and 0.40 to 0.80 fractures/m, respectively.

Cavities can be classified into two distinct types: fault-controlled and fracture-controlled cavities. The fault-controlled cavity exhibits diverse morphologies, including a narrow bar, nearly rectangular, nearly elliptical, and nearly triangular shapes. The cavity dimensions are distributed within the ranges of 6.12–22.32 m for height, 1.20–4.80 m for width, and 6.39–12.17 m for depth. The width/height and depth/height ratios fall within 0.65–0.95 and 3.04–5.21, respectively. The fracture density before, during, and after karstification is observed to be in the ranges of 0.75–2.5, 0.5–1.5, and 1.10–2.00 fractures/m, respectively. In contrast, the fracture-controlled cavity displays morphologies such as nearly rectangular, narrow bar, and nail shapes. The cavity

dimensions are in the ranges of 0.15-1.20~m for height, 0.10-1.10~m for width, and 0.35-3.9~m for depth. The aspect ratio of width to height falls between 0.26~and~0.95. The fracture density during the periods before, during, and after karstification is estimated to be in the ranges of 0.40-3.50,~0.70-2.50,~and~0.50-1.00~fractures/m, respectively. Lastly, the epi-karst cavity exhibits morphologies such as nearly circular, nearly elliptical, and long strip shapes. The cavity dimensions are mainly distributed in 0.45-2.98~m for height, 0.40-6.90~m for width, and 5.39-17.81~m for depth. The width/height and depth/height ratios are concentrated in 1.25-3.09~and~2.58-7.15, respectively. The fracture density during the periods before, during, and after karstification ranges from 0.30~to~1.50,~0.10~to~0.50,~and~0.20~to~1.50~fractures/m,~respectively.

Two distinct filling patterns were observed within the runoff zone cavity: a 5-layer filling (Type I) and a 7-layer filling. Type I filling comprised collapsed breccia, clastic deposition, chemical deposition, another layer of collapsed breccia, and an unfilled layer (from bottom to top). In Type II filling, the sequence involved hydrothermal transformation, collapsed breccia, clastic deposition, another layer of hydrothermal transformation, chemical deposition, another layer of collapsed breccia, and an unfilled layer. For fault-controlled cavities, the filling patterns were characterized by horizontal zoning, distinguishing two significant patterns: the seven-belt filling (Type I) and the five-belt filling (Type II). Type I filling included wall rock, fractured zone, chemical filling belt, hygrothermal filling belt, another chemical filling belt, fractured zone, and wall rock (from left to right). On the other hand, Type II filling comprised wall rock, fractured zone, hygrothermal filling,



Fig. 4. Typical pictures of sub categories of runoff zone cavity. (a), (b), (c), and (d) is typical outcrop picture of main stream cavity, tributary cavity, hall cavity, nespectively; (e) is oil-bearing sandstone in the main stream cavity; (f) shows the high angle oily fracture in the tributary cavity; (g) is the collapsing breccia filling in the hall cavity; (h) refers to the calcified filling in the peripheral filling.

another fractured zone, and wall rock (from left to right). In contrast, the filling pattern of epi-karst cavities was more intricate and could involve exposed carbonate rock, cliff debris, debris filling, chemical filling, collapsed breccia, and an unconformity surface. By leveraging the basic parameter knowledge of the KFCS for outcrop GKB, the fracture-cavity category could be preliminarily identified. This knowledge not only offered reliable data support but also provided effective guidance for more intricate and in-depth research on karst reservoirs.

4.3. The key mechanism knowledge of KFCS obtained by geochemical testing and water-rock simulation

4.3.1. The geochemical testing results

Three distinct types of fracture-cavity fillings were identified: cavity filling, fracture filling, and wall rock. The primary constituents of the cavity fillings included calcite, gypsum, quartz, barite, clay, plagioclase, and dolomite (Fig. 6a). Through an analysis of cutting relationships, extension characteristics, and combinational patterns, the period of fracture formation was determined (Zeng et al., 2016). Fluid inclusion testing revealed five significant tectonic activities: the Mid-Late Caledonian, Early Hercynian, Late Hercynian, Indo-Yanshanian, and Himalayan orogeny (Ren et al., 2020a, 2020b) (Fig. 6b). Calcite and gypsum constituted more than 10% of the minerals, while the remaining minerals comprised 1%–10% of the fillings. Carbon and oxygen isotope testing identified

three key filling stages (Fig. 6c). In Type I, cavity filling (Stage I) shared the same fluid source as fracture filling during the Caledonian and Early Hercynian orogenies. The δ13CPDB values ranged from -2% to -0.9%, and the $^{\delta18}O_{PDB}$ values ranged from -12%to -10%. In Type II, cavity filling (Stage II) was closely associated with fracture fillings during the Late Hercynian orogeny and the wall rock. The $^{\delta13}C_{PDB}$ values ranged from -0.8% to 0.8%, and the $^{\delta18}\mathrm{O}_{PDB}$ values ranged from -6.8% to -10%. Type III was characterized by fracture fillings during the Indo-Yanshanian and Himalayan orogenies. The $^{\delta13}C_{PDB}$ values ranged from -7% to -5% , and the $^{\delta18}O_{PDB}$ values ranged from -14% to -10.5%. Similarly, strontium isotope testing revealed three filling stages (Fig. 6d). In Type I, cavity filling (Stage I) was strongly linked to fracture fillings during the Caledonian and Early Hercynian orogenies. The ⁸⁷Sr/⁸⁶Sr values ranged from 0.710 to 0.712, and the $^{\delta 13}C_{PDB}$ values ranged from -4% to 1%. In Type II, cavity filling (Stage II) shared a similar filling environment with fractures in the Late Hercynian orogeny and the wall rock. The 87 Sr/ 86 Sr values ranged from 0.708 to 0.710, and the $^{\delta 13}C^{\text{PDB}}$ values ranged from -4% to 1‰. In Type III, the 87 Sr/ 86 Sr values ranged from 0.710 to 0.713, and the $^{\delta13}$ C_{PDB} values ranged from -6% to -5%, indicating a similar filling environment between Indo-Yanshanian and Himalayan orogeny fractures.

In the research area, the V/Cr values were predominantly concentrated between 0 and 2, with only a few instances exceeding 4.25 (Fig. 6e). Three primary sedimentary environments of the KFCS were identified: weak oxidation (2-4.5), strong oxidation (0-2),

Category		Cavity	Covity size	Fracture density	Filling features		Typical pictures (multi scale)			
Cate	egory	morphology	Cavity size	(fractures, m)	Compositons	Typical pictures	Outcrop	Core	Thin section	
	Main stream cavity	Nearly circular Nearly ellipse Like a square	Height: 0.5–4.95 m Width: 0.45–6.95 m Depth: 5.39–17.90 m Width/height: 1.15–3.09 Depth/height: 0.84–7.15	Before karst: 0.449-0.729 m Karst: 0.312-0.61 m After karst: 0.828-1.66 m	Bottom-top Unfilled Collapsed breccia Chemical deposition Clastic deposition Collapsed breccia	Carrying sand	Yijianfang profile, ellipse	Quartz fine sandstone	Quartz fine sandstone	
Runoff zone (underground river) cavity	Tributary cavity	Nearly circular Nearly ellipse Like a long strip	Height: 0.23–3.5 m Width: 0.4–6.04 m Deph: 0.57–9.93 m Width/height: 1.15–5.70 Depth/height: 0.62–6.63	Before karst: 0.15–0.5 m Karst: 0.15–0.4 m After karst: 0.2–1 m	Type I Bottom-top	Debris filling	Liuhuangou profile, ellipse, long strip	Argillaceous siltstone	Argillaceous siltstone	
Runoff zone (under	Hall cavity	Nearly ellipse Nearly triangel	Height: 8.59–13.37 m Width: 15.3–21.4 m Depth: >4 m Width/height: >1 Depth/height: 0.29–0.46	Before karst: 0.5–1.75 m Karst: 0.5–1 m After karst: 0.5–1.25 m	Unfilled Collapsed breccia Chemical deposition Hydrothermal Clastic deposition Collapsed breccia Hydro transformation	Collapse breccia	Sanjianfang profile, nearly triangle	Sandy conglomerate	Sandy conglomerate	
	Tip cavity	Nearly circular Nearly ellipse Like a long strip	Height: 0.5–1.96 m Width: 0.6–3.64 m Depth: 0.8–7.34 m Width/height: 1.2–1.86 Depth/height: 1.6–5.79	Before karst: 0.1-0.3 m Karst: 0.1-0.2 m After karst: 0.4-0.8 m	Type II	Fluorite mineral	Yijianfang profile, ellipse	Siliceous filling	Siliceous filling	
olled cavity	Fault controlled	Narrow bar Nearly rectangle Nearly ellipse Nearly triangle	Height: 6.12–22.32 m Width: 1.2–4.8 m Depth: 6.39–12.17 m Width/height: 0.65–0.95 Depth/height: 3.04–5.21	Before karst: 0.75–2.5 m Karst: 0.5–1.5 m After karst: 1.1–2 m	Type I: Wall rock + Fractured zone + Chemical filling + Hydrothermal	Calcite filling	Liuhuanggou profile, nearly rectangle	Fault breccia	Dissolved fracture	
Fault-controlled cavity	Fracture controlled	Nearly rectangle Narrow bar Nail shape	Height: 0.15–1.2 m Width: 0.1–1.1 m Depth: 0.35–3.9 m Width/height: 0.26–0.95 Depth/height: 1.5–3.46	Before karst: 0.4-3.5 m Karst: 0.7-2.5 m After karst: 0.5-1 m	Type II: Wall rock + Fractured zone + Hydro-thermal	Mega crystalline calcite	Dawangou profile, narrow bar	Dissolution along fractures oil filling	Multi dissolved fractures	
	Epi-karst cavity	Nearly circular Nearly ellipse Long strip	Height: 0.45–2.98 m Width: 0.4–6.9 m Depth: 5.39–17.81 m Width/height: 1.25–3.09 Depth/height: 2.58–7.15	Before karst: 0.3-1.5 m Karst: 0.1-0.5 m After karst: 0.2-1.5 m	Exposed carbonate rock Slope accumulation Debris filling Chemical filling Collapsed breccia Unconformity surface	Debris filling	Xekar profile, ellipse nearly circular	Developed pores, fractures, and holes, broken core	Multi dissolution-filling	

Fig. 5. The basic geological knowledge of the diverse fracture-cavity categories.

and reduction environments (>4.5). For more detailed testing data, please refer to Ren et al. (2021). Trace element testing yielded values for U, Nb, and Th, and an intersection diagram of U/Nb and Th/Nb was plotted (Fig. 6f). Two distinct fluid sources were identified in the cavity filling, fracture filling, and wall rock. Type I was significantly influenced by fluid-related enrichment (U/Nb: 0-20, Th/Nb: 0−5). Type II exhibited a high correlation with melt-related enrichment (U/Nb: 10-100, Th/Nb: 5-10). By integrating information from mineral compositions, C-O-Sr isotopes, fluid inclusion testing, and trace elements, the characteristics of the fracturecavity fluids were identified (German and Henry, 1989; Lawrence et al., 2006; Hu et al., 2010; Siahi et al., 2018). Three key filling stages were distinguished: freshwater fluid with a strong oxidizing environment, autogenous abnormally enriched hydrothermal fluid, and high-temperature hydrothermal fluid. In Stage I, the initial phase of cavity filling exhibited similarities with fracture fillings during the Caledonian and Early Hercynian orogenies, indicating a strong oxidizing environment associated with meteoric and formation karst water. In Stage II, the subsequent phase of cavity filling exhibited similarities with fracture fillings during the Late Hercynian orogeny, suggesting a weak oxidizing environment closely

related to shallow hydrothermal fluids. In Stage III, the fracture fillings during the Indo-Yanshanian period showed similarities with Himalayan fracture fillings, indicating a reduction environment significantly influenced by deep-high temperature hydrothermal fluids.

4.3.2. Water-rock numerical simulation testing

Two significant fluid types were considered in this simulation: meteoric-formation karst water (Fig. 7) and hydrothermal fluids (Fig. 8). In fractures characterized by varying apertures, dissolution initially occurred along the fracture with a larger aperture, followed by the accumulation of cavity filling in the wider aperture fracture (Fig. 7a and b). For fractures with multiple combinational patterns and similar apertures (Fig. 7c), dissolution took place along the fracture with a lower angle to the flow direction. Subsequently, cavity filling precipitated in the intersection area of different fractures with varying orientations, following the fracture orientation with the lowest angle to the flow direction (Fig. 7d). Notably, calcite fillings were concentrated at the intersection of different fractures, and the filling direction aligned with the orientation of the fracture with the larger aperture. Initially, calcite filling precipitated rapidly,

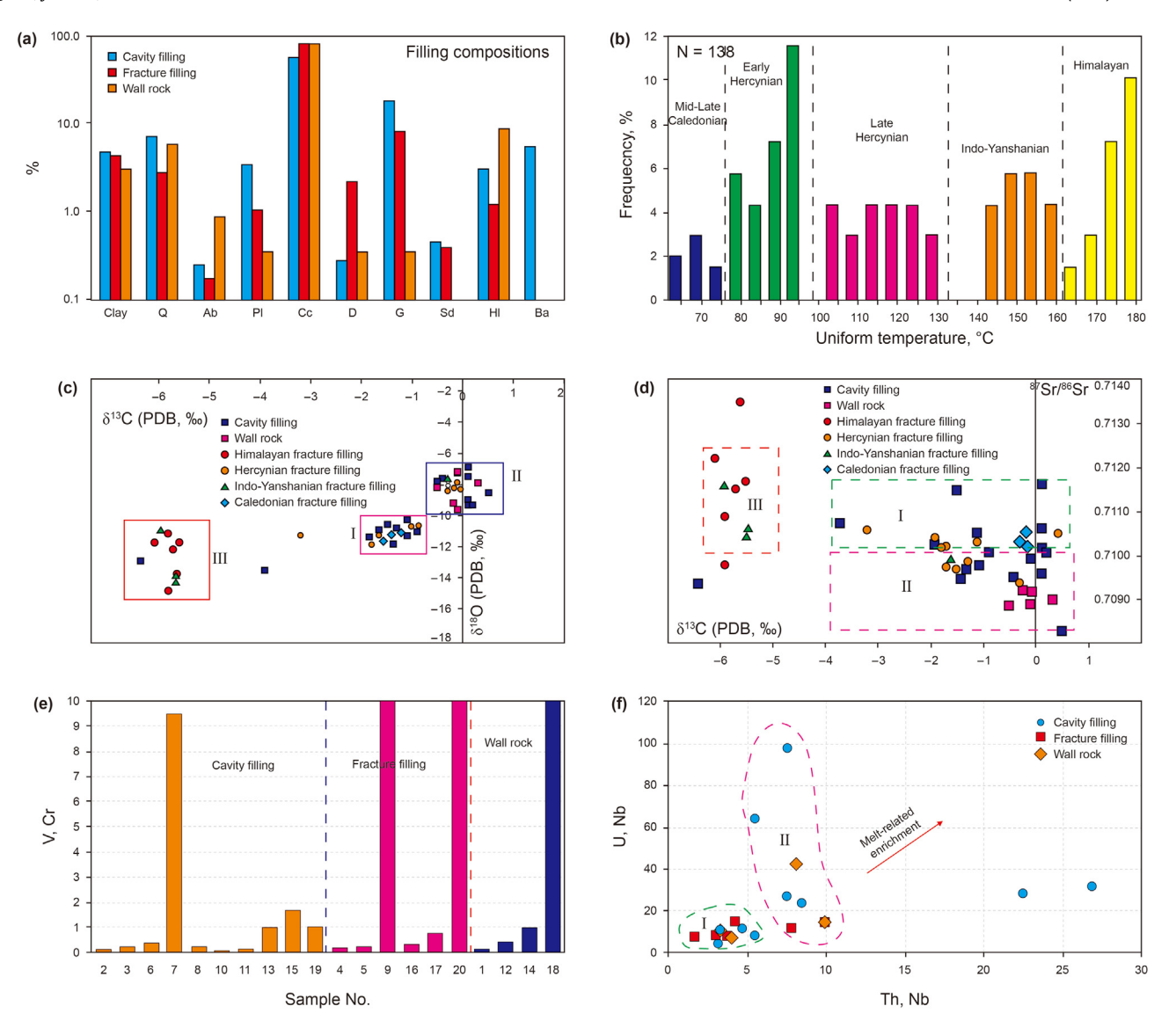


Fig. 6. The geochemical testing results of fracture-cavity fillings. (a) is the mineral compositions in the study area, where Q refers to Quartz, Ab is Potash Feldspar, Pl is Plagioclase, Cc refers to Calcite, D is Dolomite, G is Gypsum, Sd is Siderite, Hl refers to Stone salt, Ba is Barite; (b) shows the results of fluid inclusion uniform temperature; (c) refers to Carbon and Oxygen isotope testing; (d) is Strontium isotope testing; (e) is values of V/Cr in different samples; (f) refers to trace element intersection diagram of U/Nb and Th/Nb.

and then the sedimentation rate decreased until the calcite fillings reached a stable state (Fig. 7 e) (Ren et al., 2020a). Constrained by the dissolution and precipitation processes, the amount of calcite fillings in the fracture area exceeded that in the surrounding strata (Fig. 7 f). Similarly, three key stages of calcite filling were distinguished: rapid precipitation, slow precipitation, and stable stages.

In the simulation model featuring two vertical fractures with different apertures (150 m and 250 m), hydrothermal upwelling was taken into account, and the dissolution and filling processes were analyzed (Fig. 8a and b). Three key stages during hydrothermal upwelling were identified: vertical upwelling, lateral flow, and equilibrium state. In the vertical upwelling stage, fluid ascended along the initial fracture, leading to intermittent dissolution and precipitation. Calcite fillings were concentrated in the fracture core and adjacent areas. In the lateral flow stage, hydrothermal fluid flowed toward the fracture with a larger aperture, triggering dissolution and precipitation in the fracture core and areas where similar fractures intersected. During the equilibrium state, the dissolution and precipitation processes were characterized by

stable fluid flow, unchanged sediments, and fixed minerals. The dissolution and precipitation processes were scrutinized in the complex fracture-cavity system with different fluid sources. These geological results offer crucial insights into the mechanisms underlying the characterization and classification of the KFCS. Additionally, they provide valuable guidance for the exploration and development of underground karst reservoirs.

4.4. The significant representational knowledge of KFCS processed by multi mathematical methods

Utilizing multivariate linear regression, neural network techniques, and discriminant classification, significant representational parameters of the KFCS were determined, facilitating effective distinction and identification of fracture-cavity categories (Abba et al., 2017; Bozorgmanesh et al., 2020; Wang et al., 2020; Ren et al., 2020b). To illustrate, this manuscript utilized over 200 sets of various fracture-cavity categories, each comprising more than ten parameters. Each parameter was derived from a dataset of over

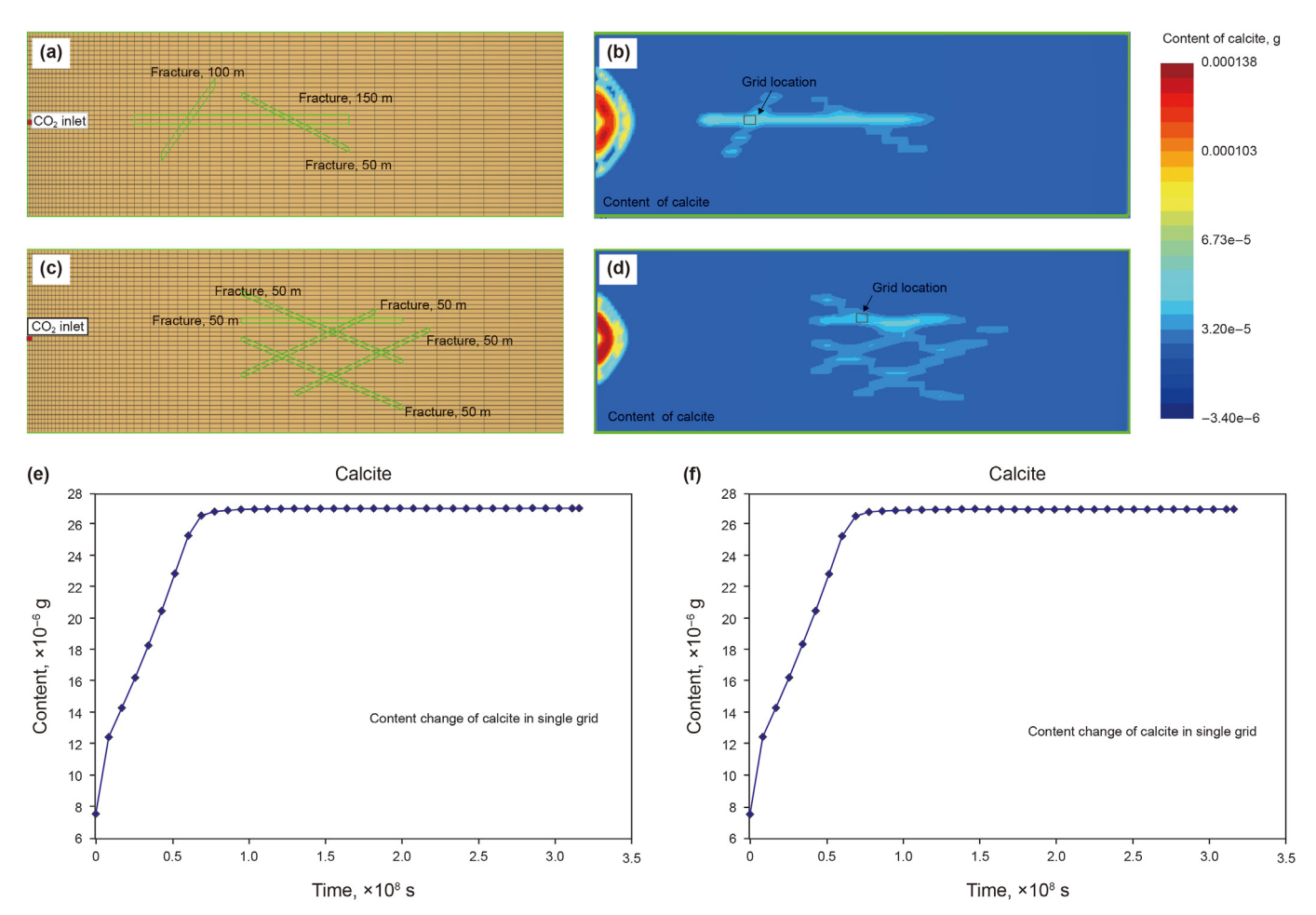


Fig. 7. The simulated results of water-rock interaction testing. (a) is established model of three fractures with various apertures, 50 m, 100 m, and 150 m; (b) shows simulated results of model of three fractures with various apertures; (c) represents the established model of complex fracture patterns; (d) shows simulated results of complex fracture patterns; (e) and (f) is changing characteristics of calcite with the simulation in the grid location in b and d, respectively.

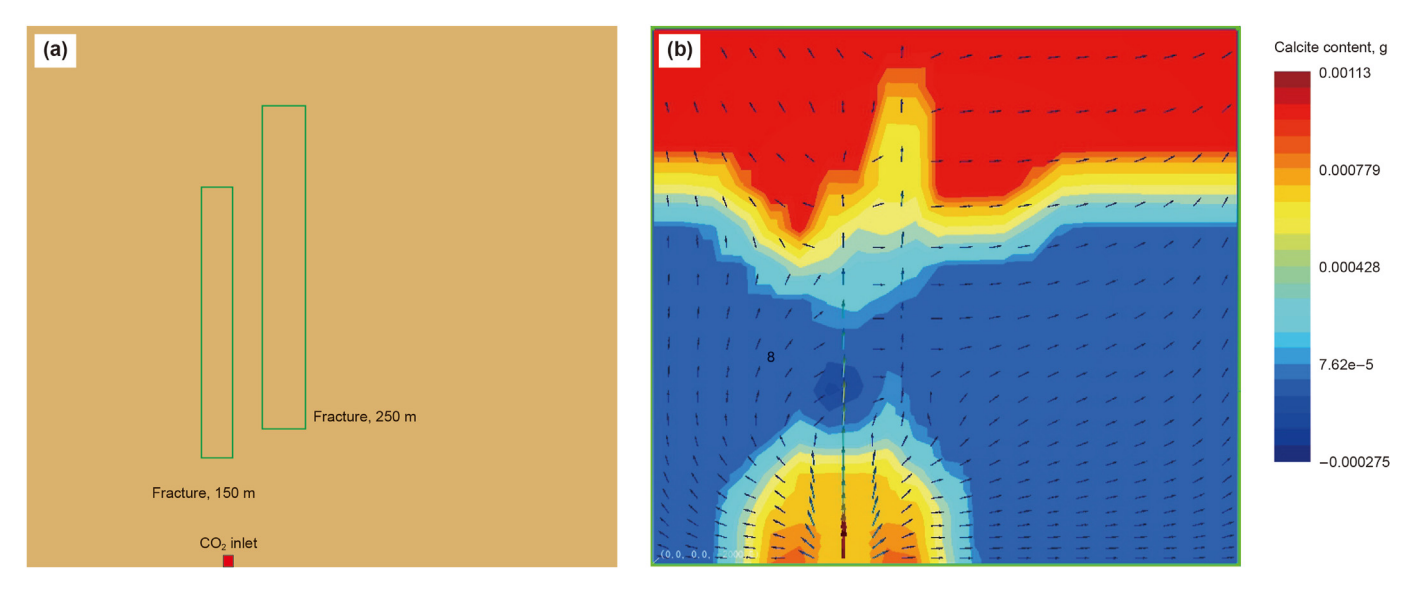


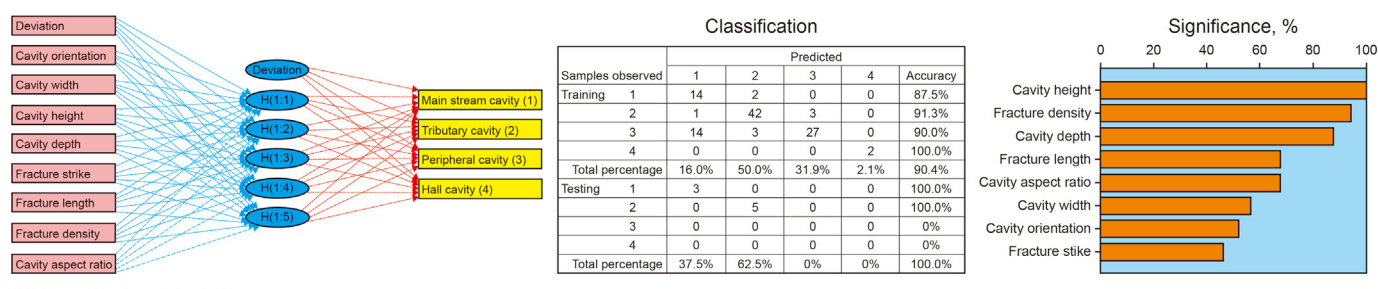
Fig. 8. (a) Shows the established model of hydrothermal upwelling with two fractures; (b) is the simulated results of hydrothermal upwelling with two fractures.

30 data points (Ren et al., 2020b for detailed data). In total, more than 60,000 data points ($200 \text{ sets} \times 10 \text{ parameters} \times 30 \text{ data points}$ per parameter) were employed to conduct a comprehensive

analysis of the significant representational knowledge of KFCS. In this manuscript, the runoff zone fracture-cavity was taken as an example to delve into the significant characterization parameters in

Correlation coefficients Coefficients Unstandardized coeffients Unstandardized coefficits Collinearity statistics Model Sig Cavity height 0.779 1.000 0.181 0.028 -0.037 -0.077 0.005 -0.939 -0.162 0.186 0.181 _0.005 Constant 3 926 9.853 ٥ 0.398 Fracture density 0.168 0.004 0.104 Cavity oientation 0.001 0.019 0.261 0.795 0.752 1.329 0.002 0.168 1.000 Cavity depth 0.038 0.085 1.633 6.663 0.069 14.399 Cavity width 0.564 0 -0 044 0.005 -0.053 -0.085 0.057 -0 142 Fracture length -0.162 -1.025 0.186 -1.210 -5.506 0 0.086 11.581 -0.939 1.000 Cavity height Cavity width Covariano 0.020 0.020 3.477E-5 3.835E--0.010 0.001 1.305E-7 Cavity depth -0.028 0.026 -0.144 -1.093 0.277 0.242 4.138 Cavity height Fracture strike 3.477E-5 4.463E-5 1.763E-6 -4.662E--1.697E--7.793E -4.073E-6 -1.816E-Fracture strike -5.222E-5 0.001 -0.003 -0.039 0.969 0.755 1.324 Fracture density 0.001 4.662E-6 0.003 3.080E-5 1.267E-5 Fracture length -0.2170.058 -0.540 -3.7480 0.201 4.987 0.001 -1.697E-7 3.080E--3 694F -0.001 Cavity depth -1.862F-6 -7.793E-7 1.267E-5 1 667E_6 0.058 0.125 1.821 0.071 0.883 1.133 0.106 Fracture density Fracture length 5.089E-6 -4.073E-6 -6.488E-6 -0.001 4.243E-6 0.003 -0.768 0.140 -0.636 -5.470 0 0.308 3.242 Cavity aspect ratio

(a) Multivariate linear regression



Cavity cat (main stream (tributary ca

(main stream (tributary ca

(b) Neural network technique

	Canonical functions			Cavity categories				
	1	2	3	1	2	3	4	
Cavity width	1.799	-1.445	-1.135	-15.818	-16.222	-14.626	10.113	
Cavity height	-2.169	2.557	3.360	32.488	32.859	28.698	-1.505	
Fracture length	0.156	0.766	-0.276	3.955	2.244	1.469	2.090	
Cavity aspect ratio	-1.885	2.021	1.430	25.751	25.447	23.032	-3.592	

Discriminant function coefficients

Classification results

	Predicted group membership								
tegories	1 (main stream cavity)	2 (tributary cavity)	3 (peripheral cavity)	4 (hall cavity)	Total				
ım cavity)	16	4	1	1	22				
avity)	6	39	14	0	59				
cavity)	0	4	32	0	36				
)	0	0	0	2	2				
ım cavity)	72.7	18.2	4.5	4.5	100.0				
avity)	10.2	66.1	23.7	0	100.0				
cavity)	0	11.1	88.9	0	100.0				
				400.0	400.0				

Eigenvalues

Function	1	2	3
Eigenvalues	2.892ª	1.130ª	0.109ª
Variance, %	70.0	27.4	2.6
Cumulative, %	70.0	97.4	100.0
Correlation	0.862	0.728	0.313

(c) Discriminant classication

Constant

1.404 -5.480

Fig. 9. The significant representational knowledge of the diverse sub categories in runoff zone karst fracture-cavity system. (a) were the results of multivariate linear regression; (b) showed the analyzed results of neural network technique; (c) referred to the results of discriminant classification.

detail (Fig. 9). Through multivariate linear regression, correlations between cavity category and parameters such as cavity orientation, width, height, depth, aspect ratio, fracture strike, length, and density were determined (Fig. 9a). For instance, the correlation coefficients between cavity aspect ratio and cavity width, and between cavity aspect ratio and cavity height, were -0.800 and 0.779, respectively. The correlation coefficient between cavity height and width was -0.939 (Fig. 9a). In general, considering the significance level (0.10), two parameters exhibited a linear relationship. Subsequently, the multivariate linear regression equation for fracture-cavity categories was established as follows,

-3.854 -37.997 -30.604 -23.221

$$y = 3.926 + 0.564x_1 - 1.025x_2 - 0.217x_3 + 0.106x_4 - 0.768x_5$$
 (1)

where y refers to the cavity type; x_1 shows the cavity width, m; x_2 refers to the cavity height, m; x_3 is the fracture length, m; x_4 represents the fracture density, /m; x_5 refers to the cavity aspect ratio.

In Eq. (1), the partial regression coefficients for cavity width, height, fracture length, density, and cavity aspect ratio were 0.564, -1.025, -0.217, 0.106, and -0.768, respectively. According to the significance level, all selected parameters were found to be relevant. With these established relationships, it became possible to distinguish the subcategories of the runoff zone fracture-cavity.

In the application of the neural network technique, a total of eight geological parameters were selected to classify the subcategories of runoff fracture-cavities (Fig. 9b). To simplify the analysis process, the main stream cavity, tributary cavity, peripheral cavity, and the hall cavity were numerically represented as 1, 2, 3, and 4, respectively. The processed samples were divided into two essential segments: the training samples (80%) and the testing samples (20%). The accuracy of the training samples reached 90.4%, while the accuracy of the testing samples achieved 100%, indicating a relatively high predictive performance. Five key parameters were identified as significant factors for classifying the fracture-cavity subcategories: cavity height, fracture density, cavity depth, fracture length, and cavity aspect ratio, with significance levels of 100%, 92%, 90%, 68%, and 68%, respectively. These findings were well-aligned with the results obtained from the multivariate linear regression analysis.

By employing the stepwise discriminant classification method, four significant geological parameters were identified to characterize the subcategories: cavity width, cavity height, fracture length, and cavity aspect ratio (Fig. 9c). The correlation coefficients of the three eigenvalue equations were 0.86, 0.73, and 0.31, respectively, indicating the cumulative classification efficiency of each subcategory. The derived discriminant function equation was used to establish the discriminant equation for the subcategories of the runoff zone cavity (Fig. 9c). Constrained by the discriminant function coefficients, the calculation equation can be expressed as follows.

$$y_1 = 1.799x_1 - 2.169x_2 + 0.156x_3 - 1.885x_4 + 1.404$$

$$y_2 = -1.445x_1 + 2.557x_2 + 0.766x_3 + 2.021x_4 - 5.480$$

$$y_3 = -1.135x_1 + 3.360x_2 - 0.276x_3 + 1.430x_4 - 3.854$$
(2)

where y_1 , y_2 , y_3 represents the canonical function; x_1 refers to the cavity width, m; x_2 shows the cavity height, m; x_3 is the fracture length, m; x_4 refers to the cavity aspect ratio.

Then the discriminant equation of sub categories was expressed as.

$$\begin{split} F_{(1)} &= -15.818x_1 + 32.488x_2 + 3.955x_3 + 25.751x_4 - 37.997 \\ F_{(2)} &= -16.222x_1 + 32.859x_2 + 2.244x_3 + 25.447x_4 - 30.604 \\ F_{(3)} &= -14.626x_1 + 28.698x_2 + 1.469x_3 + 23.032x_4 - 23.221 \\ F_{(4)} &= 10.113x_1 - 1.505x_2 + 2.090x_3 - 3.592x_4 - 73.200 \end{split}$$

where $F_{(1)}$, $F_{(2)}$, $F_{(3)}$, $F_{(4)}$ shows the main stream cavity, the tributary cavity, the peripheral cavity and the hall cavity, respectively; x_1 refers to the cavity width, m; x_2 shows the cavity height, m; x_3 is the fracture length, m; x_4 shows the cavity aspect ratio.

By applying the established discriminant formula, the predicted group membership was determined. The classification results unveiled predicted accuracy rates for the main stream cavity, tributary cavity, peripheral cavity, and hall cavity at 72.7%, 66.1%, 89.0%, and 100%, respectively. Eq. (3) enables the direct differentiation of subcategories based on the measured values of the significant geological parameters. In summary, the techniques of multivariate linear regression, neural network techniques, and discriminant classification prove to be valuable methods for guiding the subclassification of runoff cavities. Four significant representative parameters, namely cavity width, cavity height, fracture length, and cavity aspect ratio, were identified for classifying the subcategories. These methods can also be applied to classify fracture-cavity types and subcategories of fault-controlled cavities. This work not only provides greater convenience and reduces the identification time for research on runoff cavities but also contributes innovative research ideas for studying the classification of fracture-cavities, further expanding our knowledge of the significant representative characteristics of the KFCS.

Table 1The statistical table of cavity characteristics.

Phonetic code Unit Data type No Name Types Decimal places no. RDBH Qualitative description cavity number character 2 profile SSPM 3 outcrop SSLT 4 RDLX category 5 shape **RDXT** 6 filling type CTWLX filling distribution **CTWFB** 8 filling combination **CTWZH** 9 filling periods **CTWSO** 10 cavity stages RDXCQC Quantitative data 11 depth mean **SDPIZ** numerical value m depth _{max} SDZDZ 12 m 13 width min **KDZXZ** m width mean 14 KDPJZ m 15 width max **KDZDZ** m 16 height min **GDZXZ** m 17 height mean GDPIZ. 2 m 18 height $_{\rm max}$ **GDZDZ** 2 m 19 strike min ZXZXZ strike _{mean} 20 2 ZXPIZ 21 strike max ZXZDZ 2 width/height 2 22 KGB 23 depth/height SGB 2

5. Discussion and significance

5.1. The requirement analysis and platform construction of the GKB

Due to the dispersion of traditional geological knowledge across databases, professional systems, personal computers, and lengthy research reports, sharing and applying this knowledge has proven to be challenging. To tackle these challenges, various structural data tables for geological outcrops have been established, including the stratigraphic sequence table, comprehensive characteristic table of runoff cavities, and statistical table of cavity characteristics (Table 1). The statistical table of cavity characteristics encompasses six key components: name, phonetic code, data type, decimal places, unit, and standards. The geological parameters include cavity number, profile, outcrop, category, shape, depth, width, height, strike, width-to-height ratio, depth-to-height ratio, filling type, distribution, combination, periods, and cavity stages. In this manuscript, two storage types for geological data are utilized: characters and numerical values. The decimal places are standardized to two, ensuring consistency and normalization of the geological data.

Notes: RDBH indicates the first alphabet of Rongdongbianhao; SSPM shows the first alphabet of Suoshupoumian; SSLT is the first alphabet of Suoshuloutou; RDLX indicates the first alphabet of Rongdongleixing; RDXT is the first alphabet of Rongdongxingtai; CTWLX is the first alphabet of Chongtianwuleixing; CTWFB shows the first alphabet of Chongtianwufenbu: CTWZH indicates the first alphabet of Chongtianwuzuhe: CTWSO is the first alphabet of Chongtianwushigi: RDXCOC shows the first alphabet of Rongdongxingchengqici; SDPJZ, SDZDZ, and SDZXZ show the first alphabet Shendupingjunzhi, Shenduzuidazhi, Shenduzuixiaozhi, respectively; KDPJZ, KDZDZ, and KDZXZ show the first alphabet of Kuandupingjunzhi, Kuanduzuidazhi, and Kuanduzuixiaozhi, respectively; GDPJZ, GDZDZ, and GDZXZ is the first alphabet of Gaodupingjunzhi, Gaoduzuidazhi, and Gaoduzuixiaozhi, respectively; ZXPJZ, ZXZDZ, and ZXZXZ show the first alphabet of Zouxiangpingjunzhi, Zouxiangzuidazhi, and Zouxiangzuixiaozhi, respectively; KGB is the first alphabet of Kuangaobi; SGB indicates the first alphabet of Shengaobi; "/" shows no data or no definition.

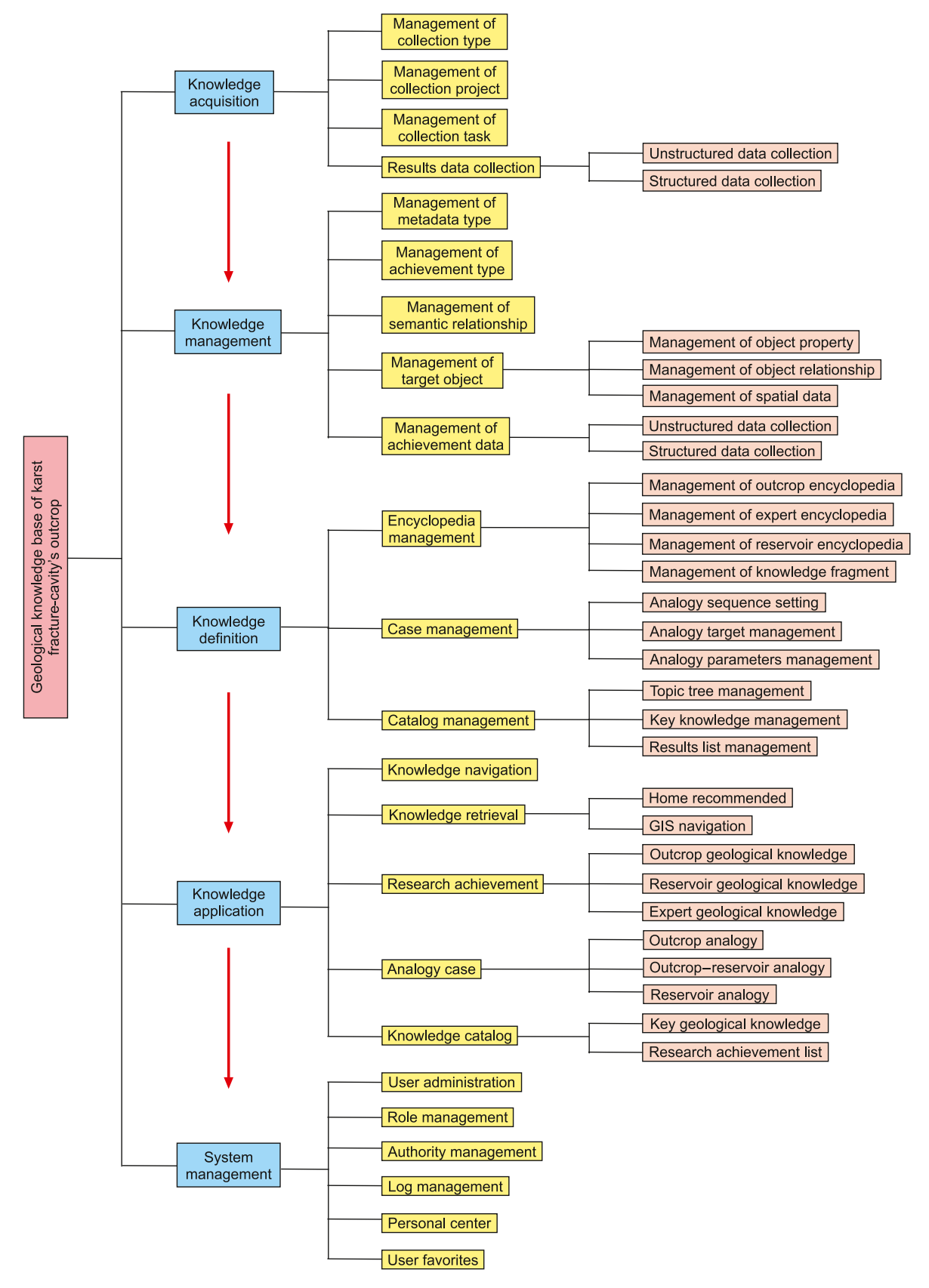


Fig. 10. The geological knowledge base compositions of karst fracture-cavity's outcrop.

Table 2The geological knowledge catalog of runoff fracture-cavity.

Level 2	Level 3	Level 4	Achievement name	Display type	Generation method	Storage method
System compositions of runoff	overview	1	description	word	unprocessed	unstructured
fracture-cavity		1	statistical table	table	unprocessed	unstructured
	geometrical characteristics of fracture-	cavity features	description	word	unprocessed	unstructured
	cavity	•	statistical table	table	mapping	structured
			outcrop figures	picture	unprocessed	unstructured
			3-D model	picture	unprocessed	unstructured
		wall rock	description	word	unprocessed	unstructured
			outcrop figures	picture	unprocessed	unstructured
		surrounding fault fracture	description	word	unprocessed	unstructured
			statistical table	table	mapping	structured
			outcrop figures	picture	unprocessed	unstructured
	fault and fracture characteristics	fault features	description	word	unprocessed	unstructured
			statistical table	table	mapping	structured
			outcrop figures	picture	unprocessed	unstructured
		fracture features	description	word	unprocessed	unstructured
			statistical table	table	mapping	structured
			histogram	picture	unprocessed	unstructured
			strike rose	picture	unprocessed	unstructured
			outcrop figures	picture	unprocessed	unstructured
		fault-fracture combination features	description	word	unprocessed	unstructured
			statistical table	table	mapping	structured
			histogram	picture	unprocessed	unstructured
			outcrop figures	picture	unprocessed	unstructured
	fracture cavity filling characteristics	filling types	description	word	unprocessed	unstructured
			pattern	picture	unprocessed	unstructured
			outcrop figures	picture	unprocessed	unstructured
		filling features	description	word	unprocessed	unstructured
			testing data	table	mapping	structured
			statistic figure	picture	unprocessed	unstructured
			micro figure	picture	unprocessed	unstructured
			environment	word	unprocessed	unstructured
		filling stages	description	word	unprocessed	unstructured
			testing data	table	mapping	structured
			figures	picture	unprocessed	unstructured
	combinational characteristics of fracture-cavity	cavity combination	description	word	unprocessed	unstructured
			pattern	picture	unprocessed	unstructured
		fault-cavity combination	outcrop figures	picture	unprocessed	unstructured
			description	word	unprocessed	unstructured
			feature table	table	mapping	structured
			statistic figure	picture	unprocessed	unstructured
			pattern	picture	unprocessed	unstructured
		fault-cavity combination Multi-layers cavity combination	Outcrop figures	picture	unprocessed	unstructured
			description	word	unprocessed	unstructured
			pattern	picture	unprocessed	unstructured
			Outcrop figures	•	unprocessed	unstructured

Inspired by the Baidu Encyclopedia platform and in collaboration with Jurassic Software company, the structure and composition of the Geological Knowledge Base (GKB) have been developed. Five key components have been identified: knowledge acquisition, management, definition, application, and system management (Fig. 10). Knowledge acquisition encompasses type management, project management, task management, and data collection of results. Knowledge management consists of five sub-components: metadata type, achievement type, semantic relationship, target object, and achievement data. Knowledge definition includes encyclopedia management, case management, and catalog management. These three aspects were essential for constructing an effective geological knowledge base. Through standardized and normalized knowledge acquisition and definition, basic geological knowledge, key mechanism knowledge, and significant representation knowledge of each fracture-cavity category can be directly and effectively distinguished.

Similarly, knowledge application comprises navigation, retrieval, research achievements, analogy cases, and knowledge catalog (Fig. 10). System management consists of user administration, role management, authority management, log management,

personal center, and user favorites. By editing display templates, various search keywords and interface requirements can be configured to meet the needs of different field developments and geologists. Metadata types and values allow for searching corresponding geological knowledge and data. To facilitate convenient, quick, and efficient retrieval of geological knowledge, six key buttons have been configured: homepage recommendation, research awareness, knowledge catalog, definition, management, and collection. These buttons enable efficient searching, editing, uploading, modification, and addition of geological data and knowledge, reducing redundant and tedious work.

5.2. The data storage and applications of the GKB

By leveraging an internet encyclopedia, research outcomes could be obtained quickly, accurately, and comprehensively. The GKB storage outline comprised eight significant components: outcrop profile description, strata features, structural features, sedimentary features, reservoir features, figure list, video list, and digital model. For instance, in the case of runoff fracture-cavities, four key compositions were determined: geometrical

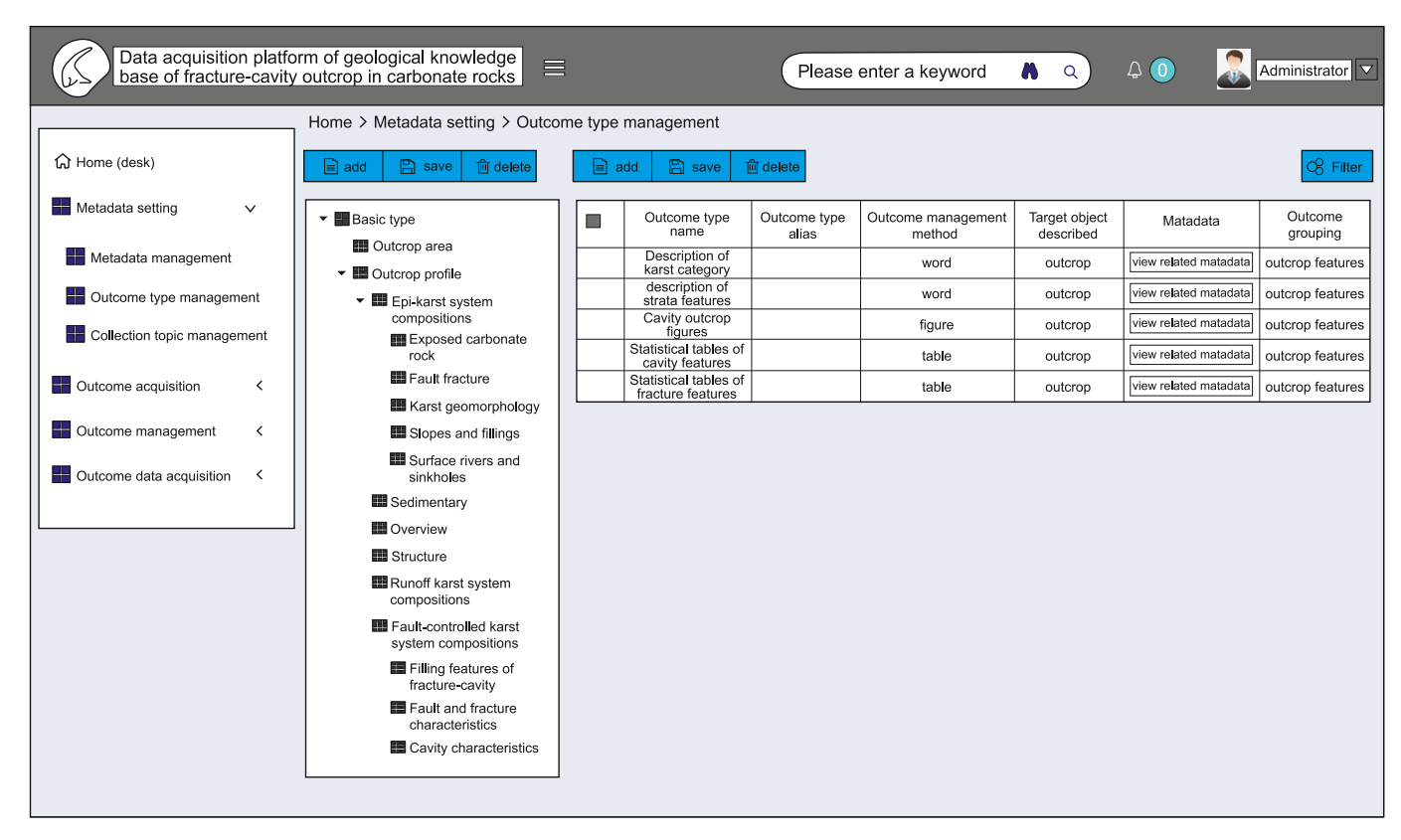


Fig. 11. The outcome type management interface of outcrop geological knowledge base for fracture cavity reservoir (all the data and knowledge were edited in the display platform of knowledge base, similar to Baidu Encyclopedia).

characteristics, fault and fracture characteristics, fracture-cavity filling characteristics, and combinational characteristics (Table 2). Through detailed exhibitions, the distinctive characteristics of different fracture-cavity categories could be intuitively discerned. Given the complexity and specificity of geological knowledge compositions, an editing function was added to supplement corresponding geological label properties based on industry requirements. The knowledge system was sorted and organized, determining the outcome type unit for each knowledge (Fig. 11). With professional collaboration, the collection of outcrop knowledge results could be swiftly completed. By reading selected files and making batch metadata modifications, the rapid collection of knowledge achievements was achieved.

Considering the diverse formats of outcomes, the knowledge definition tool was developed with display components for images. text, tables, PDFs, multi-images, videos, and 3D data. The geological knowledge encyclopedia was generated using the modified template (Fig. 12), taking the runoff fracture-cavity and Yijianfang profile as examples. To facilitate the comparison of similar geological outcrops, the case management module was developed to establish an analogy knowledge system and case entry. As a result, customization and maintenance of the knowledge catalog were achieved. In the application module of the outcrop GKB, research achievements related to the target object could be easily and accurately searched based on the basic property parameters. Leveraging the knowledge system, specific geological knowledge fragments were extracted from the geological database, providing insights into the study status of various fracture-cavity types. Moreover, a web display function for 3D digital models was implemented, allowing effective integration with the outcrop GKB. This facilitated the construction of a GIS navigation function to locate corresponding geological targets, showcasing their basic parameter knowledge, key mechanism knowledge, and significant representational knowledge directly. Furthermore, establishing internal relationships among knowledge fragments supported efficient knowledge search, while extracting professional logical relationships among different geological targets uncovered valuable insights into the professional coupling of diverse data.

5.3. Developmental characteristics of underground fracture-cavity and its significance

Through outcrop observations, two distinct dissolution and filling types were identified: vertical and horizontal dissolution (Fig. 13a). Vertical dissolution primarily occurred along faults or large-scale fractures, resulting in narrow, elongated, and large cavities. The fracture-cavities exhibited a consistent orientation with the extension of the fault, displaying a vertically beaded and gourd-like erosion pattern. Horizontal dissolution occurred along formation interfaces or horizontal fractures, leading to flat, elongated, and small cavities. The location of the fracture-cavities was closely related to lithological variations and patterns of fracture combinations, indicating intermittent and differential erosion horizontally. Underground fracture-cavities, primarily comprising main stream cavities and hall cavities, represent significant reservoir spaces in the river mound valley (Fig. 13b). The scale of fracture-cavities was greatly influenced by water table fluctuations, resulting in their expansion. For example, in well TK730, four distinct water table rises were identified at depths of 5578.5 m, 5573.0 m, 5568.5 m, and 5565.0 m, revealing an intermittent rising pattern. The porosity of sedimentary fillings ranged from 12% to 25%, and permeability fell within the range of 100-1000 Md. The porosity of collapse fillings ranged from 16% to 18%, with permeability varying between 1 and 1000 Md. The porosity of chemical

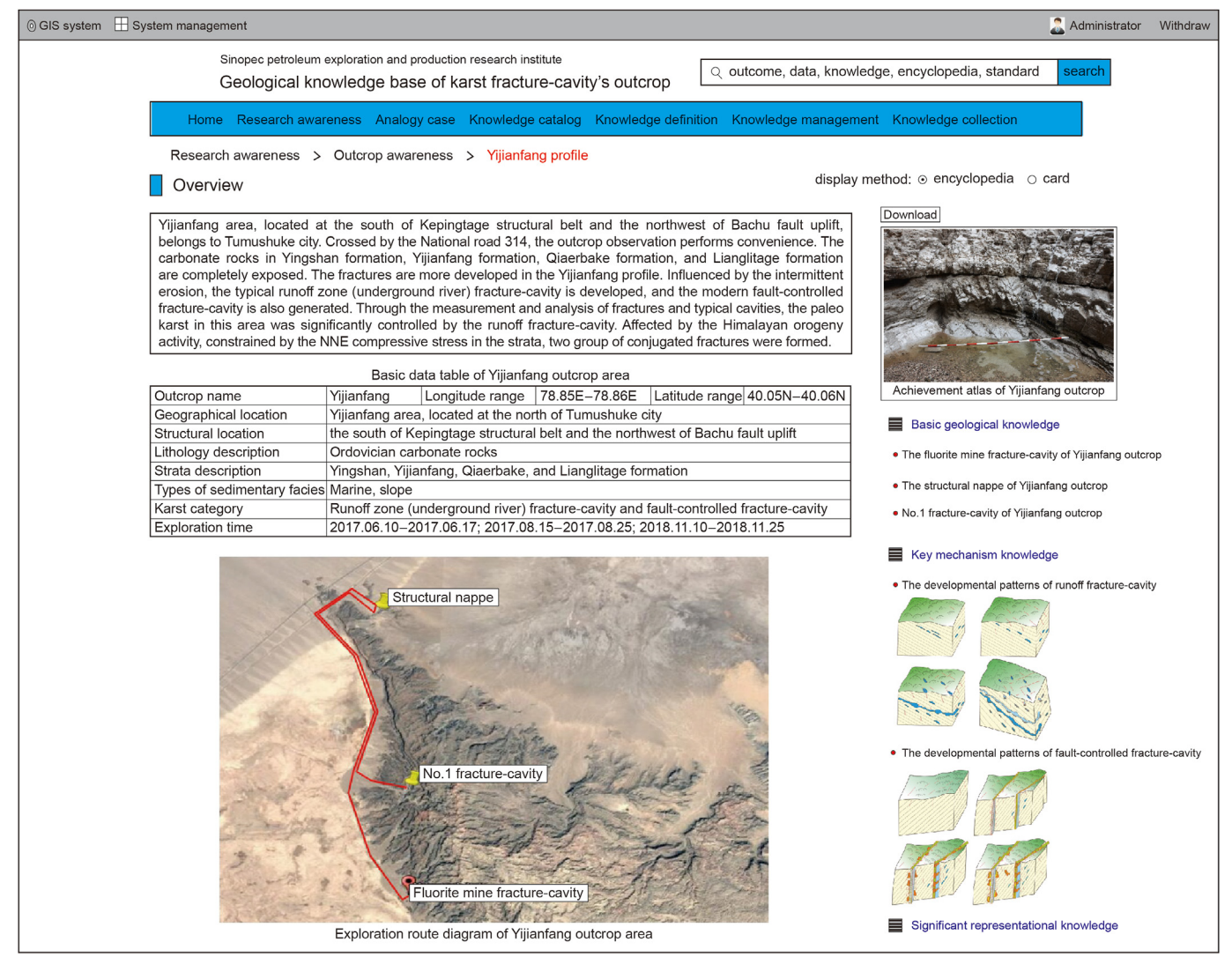


Fig. 12. The research and understanding interface of outcrop geological knowledge base for fracture-cavity reservoir (Yijianfang outcrop area).

fillings was less than 2%, and permeability was less than 10 Md.

Due to minimal compression, the main stream cavities and hall cavities served as important reservoirs with favorable physical properties. Interestingly, fracture-cavities were concentrated at the top of faults, extending over the fault plane. Horizontally, the fracture-cavities exhibited a contiguous distribution, particularly in the intersection area of various faults. Vertically, the erosion direction was significantly influenced by the fault and the combination of multiple fractures. Initially, erosion occurred along horizontal fractures and formation interfaces. As the fault developed, cavities were extended by the fault throw and dip angle, leading to a change in the direction of dissolution and filling along the fault surface and the development of fracture-cavities along new interfaces. The scale of cavities near the fault was larger than those further away. The water table could be altered due to the high activity of faults with steep dip angles (Fig. 13b). Hydrothermal filling was concentrated in the fault area, while cliff debris was distributed at the top of carbonate rocks. In areas where multiple combined fractures existed, the vertical extension and shape of the cavities were altered. Small-scale cavities were primarily developed in the intersection area of multiple fractures, with their orientation consistent with the fracture with a larger aperture. This implies that the outcrop GKB can effectively and accurately guide research on fracture-cavity characteristics in underground reservoirs in the Tahe oilfield.

The thickness of deposit fillings was primarily concentrated between 5 and 15 m, with few exceeding 15 m. Areas with greater thickness were mainly found in the southeastern part of the T615 unit, particularly in the vicinity of the river mound valley and karst basin (Fig. 13c). The thickness of collapsed fillings was mainly distributed between 4 and 12 m, with few exceeding 12 m. The most extensive development of collapsed fillings occurred in adjacent areas, such as well TK734. Similarly, the unfilled rate was predominantly distributed between 0% and 90%, with few values falling below 10%. The lowest unfilled rates were concentrated in the southeastern area of the T615 unit, especially in the intersection area of the northwest-striking fault and northeast-striking fault. Furthermore, the relationship between cumulative production and the fracture-cavity complex was analyzed (Fig. 13c). High cumulative production (>100,000 m³) was observed in areas with a developed fracture-cavity complex (10-20 m). The cumulative oil production ranged from 32,000 to 46,000 t, with an effective fracture-cavity reservoir thickness of 10-20 m. The presence of fault-controlled fracture-cavity reservoirs indicated high-yield

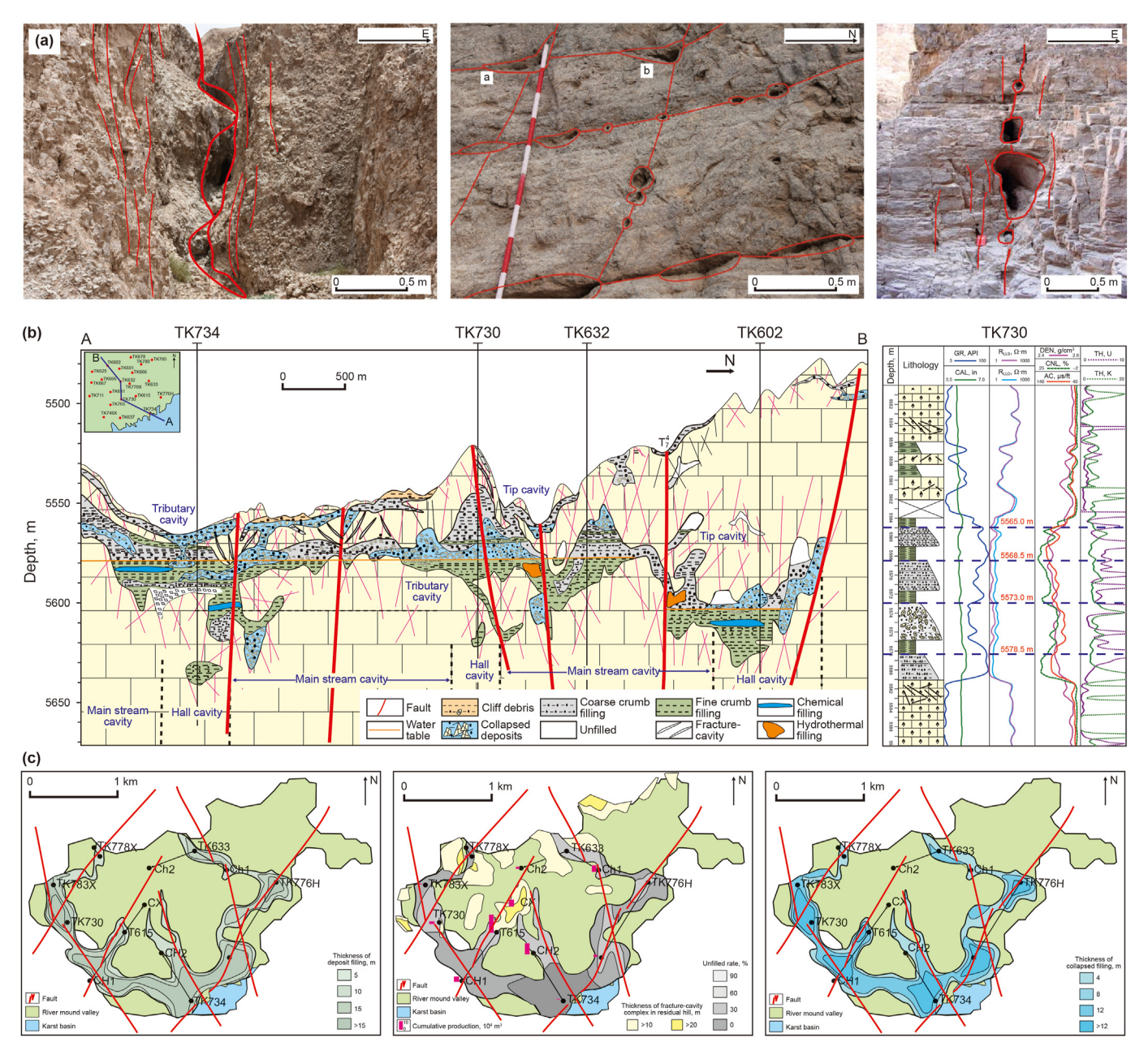


Fig. 13. The analogy research diagram of outcrop and underground fracture-cavity. (a) is the significant dissolution and filling in outcrop fracture-cavity; (b) refers to the underground fracture-cavity compositions in the well-connected profile; (c) shows the equal thickness map of different filling types in the T615 unit, Tahe oilfield.

storage space, leading to increased oil production in the middle area of the T615 unit (Fig. 13c). Consequently, the novel fracture-cavity reservoir outcrop geological knowledge base construction method could provide a new way to conduct complex and in-depth research on the exploration and development of fracture-cavity reservoirs.

6. Conclusions

In conclusion, we employed advanced techniques, including multi-scale characterization, geochemical testing, and mathematical analyses, to synthesize comprehensive knowledge about the Karst Fracture-Cavity System (KFCS). This facilitated a comparative analysis between outcrop and underground reservoir developmental characteristics, enhancing the dissemination and

application of geological insights.

- (1) We developed cutting-edge technology for acquiring and processing 3D geological data through extensive observations and studies of karst outcrops. Macro geological data were collected and standardized using techniques such as outcrop observations, core statistics, unmanned aerial vehicle scanning, and high-resolution cameras. Additionally, micro data were obtained and normalized using methods like thin-section analysis and electron scanning imaging.
- (2) The Geological Knowledge Base (GKB) comprises three key components: basic parameter knowledge, key mechanism knowledge, and significant representational knowledge. Basic parameter knowledge involves classified parameters for different fracture-cavity categories obtained through fine

- characterization techniques. Key mechanism knowledge is derived from isotope-trace element testing and water-rock interaction numerical simulation. Significant representational knowledge includes quantitative classification parameters for various fracture-cavity categories.
- (3) The construction of GKB involves two crucial steps: platform construction and data storage. The platform components knowledge acquisition, management, definition, application, and system management - significantly enhance knowledge efficiency. Data storage follows three key stages: summary statistics, format conversion, and normalized processing.
- (4) Innovative analogy research, using the T615 unit in Tahe oilfield as an example, demonstrated strong consistency in the developmental characteristics of fracture-cavities between outcrops and underground reservoirs. Areas with developed fracture-cavity complexes (10–20 m) exhibited high cumulative production (>100,000 m³), with cumulative oil production ranging from 32,000 to 46,000 t. The outcrop GKB construction method can be broadly applied to fracture-cavity reservoirs worldwide, encompassing diverse regions, layers, and formations.

CRediT authorship contribution statement

Qi-Qiang Ren: Conceptualization, Formal analysis, Methodology, Writing — original draft, Writing — review & editing. **Jin-Liang Gao:** Formal analysis, Validation. **Peng Zhu:** Data curation, Investigation. **Meng-Ping Li:** Conceptualization, Investigation, Methodology. **Jian-Wei Feng:** Funding acquisition, Supervision. **Qiang Jin:** Software, Supervision. **San Zhang:** Methodology, Visualization.

Declaration of competing interest

The authors declare that they have no known competing financial interests or personal relationships that could have appeared to influence the work reported in this paper.

Acknowledgement

This research was supported by the Major Scientific and Technological Projects of CNPC under grant ZD2019-183-006, the National Science and Technology Major Project of China (2016ZX05014002-006), and the National Natural Science Foundation of China (42072234, 42272180). The authors would like to express their gratitude to all the individuals who provided support in terms of data, testing, and analyses. Special thanks are extended to the anonymous reviewers whose valuable comments have greatly contributed to improving the quality of our manuscript.

References

- Abba, S.I., Hadi, S., Abdullahi, J., 2017. River water modeling prediction using multilinear regression, artificial neural network, and adaptive neuro-fuzzy inference system techniques. Procedia Comput. Sci. 120, 75–82. https://doi.org/10.1016/ i.procs.2017.11.212.
- Amirjan, M., Bozorg, M., 2018. Properties and corrosion behavior of Al based nanocomposite foams produced by the sintering-dissolution process. Int. J. Miner. Metall. Mater. 25 (1), 94–101. https://doi.org/10.1007/s12613-018-1551-5
- Araújo, R.E.B., La, B.V., Rustichelli, A., Bezerra, F.H., Xavier, M., Audra, P., Barbosa, J.A., Antônino, A.C.D., 2021. Structural and sedimentary discontinuities control the generation of karst dissolution cavities in a carbonate sequence, Potiguar Basin, Brazil. Mar. Petrol. Geol. 123, 104753. https://doi.org/10.1016/j.marpetgeo.2020.104753.
- Bagni, F.L., Erthal, M.M., Tonietto, S.N., Maia, R.P., Bezerra, F.H., Balsamo, F., Córdoba, V.C., Souza, F.G., Brod, J.A., Fernandes, C.P., Fonseca, J.P.T., 2022. Karstified layers and caves formed by superposed epigenic dissolution along subaerial unconformities in carbonate rocks—Impact on reservoir-scale

permeability. Mar. Petrol. Geol. 105523. https://doi.org/10.1016/j.marpetgeo.2022.105523.

- Bozorgmanesh, H., Hajarian, M., Chronopoulos, A.T., 2020. Interval tensors and their application in solving multi-linear systems of equations. Comput. Math. Appl. 79 (3), 697–715. https://doi.org/10.1016/j.camwa.2019.07.024.
- Cai, Z.X., Zhang, H., Qi, L.X., Yun, L., Cao, Z.C., Sha, X.G., 2020. Types and characteristics of karst hydrogemorphologic architecture in the middle-lower ordovician, Tarim Basin. Acta Petrol. Sin. 41 (1), 43–58. https://doi.org/10.7623/svxb202001004.
- Castillo, M.V., Mann, P., 2006. Deeply buried, early cretaceous paleokarst terrane, Southern Maracaibo basin, Venezuela. AAPG Bull. 90 (4), 567–579. https://doi.org/10.1306/10120505034.
- Cavailhes, T., Gillet, H., Guiastrennec, F.L., Mulder, T., Hanquiez, V., 2022. The abyssal giant sinkholes of the Blake Bahama Escarpment: evidence of focused deepocean carbonate dissolution. Geomorphology 398, 108058. https://doi.org/ 10.1016/j.geomorph.2021.108058.
- Chen, Q.L., Zhao, Y.Q., Li, G.R., Chu, C.L., Wang, B., 2012. Features and controlling factors of epigenic karstification of the Ordovician carbonates in Akekule arch, Tarim basin. J. Earth Sci. 23 (4), 506–515. https://doi.org/10.1007/s12583-012-0271-4
- Chen, S.Y., Wang, Y.J., Guo, J.Y., He, Q.L., Yin, X.R., 2021. Multi-scale evaluation of fractured carbonate reservoir and its implication to sweet-spot optimization: a case study of Tazhong oilfield, Central Tarim Basin, China. Energy Rep. 7, 2976–2988. https://doi.org/10.1016/j.egyr.2021.05.017.
- Firme, A.L.P., Quevedo, R.J., Roehl, D., Pereira, L.C., Cazarin, C.L., 2021. Mechanical behavior of carbonate reservoirs with single karst cavities. Geomech. Energy Environ. 25, 100209. https://doi.org/10.1016/j.gete.2020.100209.
- Fu, X.F., Su, X.C., Gong, L., Wang, Q.Q., Gao, S., Xie, Z.H., 2023. Control of faults and fractures on shale oil enrichment. Geoenergy Sci. Eng. 228, 212080. https:// doi.org/10.1016/j.geoen.2023.212080.
- German, C.R., Henry, E., 1989. Rare earth elements in Saanich Inlet, British Columbia, a seasonally anoxic basin. Geochem. Cosmochim. Acta 53 (10), 2561–2571. https://doi.org/10.1016/0016-7037(89)90128-2.
- González-Esvertit, E., Canals, A., Bons, P.D., Casas, J.M., Gomez-Rivas, E., 2022. Compiling regional structures in geological databases: the Giant Quartz Veins of the Pyrenees as a case study. J. Struct. Geol. 163, 104705. https://doi.org/10.1016/ i.isg.2022.104705.
- González-Esvertit, E., Alcalde, J., Gomez-Rivas, E., 2023. IESDB-The Iberian evaporite structure database. Earth Syst. Sci. Data 15 (7), 3131–3145. https://doi.org/10.5194/essd-15-3131-2023.
- Haeri, A.O., Al-Aasm, I., Coniglio, M., 2013. Fracture mineralization and fluid flow evolution: an example from Ordovician-Devonian carbonates, southwestern Ontario, Canada. Geofluids 13 (1), 1–20. https://doi.org/10.1111/gfl.12003.
- Hassanzadeh, A., Vázquez-Suñé, E., Corbella, M., Criollo, R., 2022. An Automatic Geological 3D Cross-Section Generator: Geopropy, an Open-Source Library. Environmental Modelling & Software, 105309. https://doi.org/10.1016/ j.envsoft.2022.105309.
- He, Z.L., Peng, S.T., Zhang, T., 2010. Controls on reservoir formation in Ordovician of Tahe oilfield, Tarim basin, and combinational genetic mechanism. Oil Gas Geol. 31 (6), 743–752. https://doi.org/10.11743/ogg20100607.
- He, Z.L., Sun, J.F., Guo, P.H., Wei, H.H., Lyu, X.R., Han, K.L., 2021. Construction method of carbonate reservoir knowledge base and its application in fracture-cavity reservoir geological modeling. Petrol. Explor. Dev. 48 (4), 710–718. https:// doi.org/10.1016/S1876-3804(21)60069-1.
- Hu, W.X., Chen, Q., Wang, X.L., Cao, J., 2010. REE models for the discrimination of fluids in the formation and evolution of dolomite reservoirs. Oil Gas Geol. 31 (6), 810–818. https://doi.org/10.1016/S1876-3804(11)60008-6.
- Jia, P., Li, W., Li, M., Deng, S.H., Lu, Y.Z., Li, X., Fan, R., Liu, X., 2017. Characteristics of carbon and oxygen isotopes and their significance of the Cambrian Xixiangchi Group carbonate rocks in eastern Sichuan Basin. J. Palaeogeoge 19 (3), 503–512. https://doi.org/10.7605/gdlxb.2017.03.039.
- Jin, Z.J., Zhu, D.Y., Meng, Q.Q., Hu, W.X., 2013. Hydrothermal activities and influences on migration of oil and gas in Tarim basin. Acta Petrol. Sin. 29, 1049–1058. https://doi.org/10.1134/S1075701513020025.
- Jin, Q., Cheng, F.Q., Tian, F., 2017. Identification of fracture-vug complex from karsted carbonates and its significance in petroleum geology. J. China Univ. Petrol. (Edition of Nat. Sci.) 41 (3), 49–55. https://doi.org/10.3969/j.issn.1673-5005.2017.03.006.
- Lawrence, M.G., Greig, A., Collerson, K.D., Kamber, B.S., 2006. Rare earth element and yttrium variability in South East Queensland waterways. Aquat. Geochem. 12 (1), 39–72. https://doi.org/10.1007/s10498-005-4471-8.
- Li, B.G., Gao, R.S., 2014. Characteristics and main controlling factors of karst caves in the southern margin of Kepingtage tectonic belt, Tarim Basin. Geoscience 1 (2), 149–155. https://doi.org/10.3969/j.issn.1000-8527.2014.01.014, 1000-8527(2014)01-0149-07.
- Li, Y., Yu, Q.Y., Liu, P.C., Wang, Q., Zhang, Q., Zhang, J., Zhao, F.L., 2022. Rate transient analysis of fractured-caved carbonate reservoirs under different cave connecting modes. J. Petrol. Sci. Eng. 208, 109524. https://doi.org/10.1016/ j.petrol.2021.109524.
- Loucks, R.G., 1999. Paleocave carbonate reservoirs: origins, burial-depth modifications, spatial complexity, and reservoir implications. AAPG (Am. Assoc. Pet. Geol.) Bull. 83 (11), 1795–1834. https://doi.org/10.1306/E4FD426F-1732-11D7-8645000102C1865D.
- Lu, Z.Y., Chen, H.H., Feng, Y., Wu, Y., Xiong, W.L., Shang, P., 2015. Evidences of multiepisodically paleo-fluid flow and its significance in Ordovician of Guchengxu

uplift, Tarim basin. Earth Sci. J. China Univ. Geosci. 40, 1529–1537. https://doi.org/10.3799/dgkx.2015.137.

- Lyu, X.R., Sun, J.F., Wu, X.W., Wei, H.H., Xiao, F.Y., Ma, C.Y., Song, C.Z., 2021. Internal architecture characterization of fractured-vuggy carbonate reservoirs: a case study on the Ordovician reservoirs, Tahe Unit S67, Tarim Basin. Oil Gas Geol. 42 (3), 728–737. https://doi.org/10.11743/ogg20210317.
- Ma, Y.S., Cai, X.Y., Yun, L., Li, Z.J., Li, H.L., Deng, S., Zhao, P.R., 2022. Practice and theoretical and technical progress in exploration and development of Shunbei ultra-deep carbonate oil and gas field, Tarim Basin, NW China. Petrol. Explor. Dev. 49 (1), 1–20. https://doi.org/10.1016/S1876-3804(22)60001-6.
- Mao, C., Zhong, J.H., Wang, Y.Z., Wei, H.H., Shao, Z.F., Liu, J.L., Liu, J.J., 2018. Origin of chemical fillings in ordovician fracture-cave of Bachu uplift in Tarim Basin. J. China Univ.Petrol. 42 (6), 50–58. https://doi.org/10.3969/j.issn.1673-5005.2018.06.006.
- Mazzullo, S.J., 2004. Overview of porosity evolution in carbonate reservoirs. Kansas Geol. Soc. Bull. 79 (1–2), 1–19. https://doi.org/10.3997/2214-4609.20142634.
- Méndez, J.N., Jin, Q., González, M., Zhang, X.D., Lobo, C., Boateng, C.D., Zambrano, M., 2020. Fracture characterization and modeling of karsted carbonate reservoirs: a case study in Tahe oilfield, Tarim Basin (western China). Mar. Petrol. Geol. 112, 104104. https://doi.org/10.1016/j.marpetgeo.2019.104104.
- Méndez, J.N., Jin, Q., Zhang, X.D., González, M., Kashif, M., Boateng, C.D., Zambrano, M., 2021. Rock type prediction and 3D modeling of clastic paleokarst fillings in deeply-buried carbonates using the Democratic Neural Networks Association technique. Mar. Petrol. Geol. 127, 104987. https://doi.org/10.1016/i.marpetgeo.2021.104987.
- Negahdari, Z., Khandoozi, S., Ghaedi, M., Malayeri, M.R., 2022. Optimization of injection water composition during low salinity water flooding in carbonate rocks: a numerical simulation study. J. Petrol. Sci. Eng. 209, 109847. https://doi.org/10.1016/j.petrol.2021.109847.
- Ning, C.Z., Sun, L.D., Zeng, H.L., Hu, S.Y., Li, Y., Pan, W.Q., Yao, Z.X., Yuan, W.F., Sun, C.H., 2022. Characteristics of collapsed subsurface paleokarst systems and controlling factors of subsurface paleokarst development in the Lianglitage Formation, Halahatang oilfield, Tarim Basin, NW China. Mar. Petrol. Geol. 137, 105488. https://doi.org/10.1016/j.marpetgeo.2021.105488.
- Ren, Q.Q., Jin, Q., Feng, J.W., Li, M.P., Du, H., 2020a. Mineral filling mechanism in complex carbonate reservoir fracture system: enlightenment from numerical simulation of water-rock interaction. J. Petrol. Sci. Eng. 195, 107769. https:// doi.org/10.1016/j.petrol.2020.107769.
- Ren, Q.Q., Jin, Q., Feng, J.W., Du, H., 2020b. Design and construction of the knowledge base system for geological outfield cavities classifications: an example of the fracture-cavity reservoir outfield in Tarim basin, NW China. J. Petrol. Sci. Eng. 194, 107509. https://doi.org/10.1016/j.petrol.2020.107509.
- Ren, Q.Q., Feng, J.W., Ma, J., Du, H., 2021. Filling provenance in fracture cavity formation within aksu area, Tarim Basin, NW China: indicators from major and trace element, carbon-oxygen, and strontium isotope compositions. Lithosphere (Special 1), 5559457. https://doi.org/10.2113/2021/5559457.
- Rongier, G., Collon-Drouaillet, P., Filipponi, M., 2014. Simulation of 3D karst conduits with an object-distance based method integrating geological knowledge. Geomorphology 217, 152–164. https://doi.org/10.1016/j.geomorph.2014.04.024.
- Shi, S.Y., Hu, S.Y., Liu, W., Liang, D.X., Qiao, H., 2014. Ordovician paleokarst cave system and it's controlling factor in Xekar, Tarim Basin. Nat. Sci. Geosci. 26 (2), 208–217. https://doi.org/10.11764/j.issn.1672-1926.2014.02.0167.
- Siahi, M., Hofmann, A., Master, S., Wilson, A., Mary, C., 2018. Trace element and stable (C, O) and radiogenic (Sr) isotope geochemistry of stromatolitic carbonate rocks of the Mesoarchaean Pongola Supergroup: implications for

- seawater composition. Chem. Geol. 476, 389-406. https://doi.org/10.1016/j.chemgeo.2017.11.036.
- Tian, F., Jin, Q., Lu, X.B., Lei, Y.H., Zhang, L.K., Zheng, S.Q., Zhang, H.F., Rong, Y.S., Liu, N.G., 2016. Multi-layered Ordovician paleokarst reservoir detection and spatial delineation: a case study in the Tahe Oilfield, Tarim Basin, Western China. Mar. Petrol. Geol. 69, 53–73. https://doi.org/10.1016/j.marpetgeo.2015.10.015.
- Wang, Y., Hou, J.R., Tang, Y., Song, Z.J., 2019. Effect of vug filling on oil-displacement efficiency in carbonate fractured-vuggy reservoir by natural bottom-water drive: a conceptual model experiment. J. Petrol. Sci. Eng. 174, 1113–1126. https://doi.org/10.1016/j.petrol.2018.12.014.
- Wang, X.Z., Che, M.L., Wei, Y.M., 2020. Neural network approach for solving nonsingular multi-linear tensor systems. J. Comput. Appl. Math. 368, 112569. https://doi.org/10.1016/j.cam.2019.112569.
- Xie, J., Guo, G.A., Tang, Q.S., Peng, X., Deng, H., Xu, W., 2021. Key technologies for the efficient development of ultra-deep ancient dolomite karst gas reservoirs: a case study of the Sinian Dengying Formation gas reservoir in the Anyue gas field of the Sichuan Basin. Nat. Gas. Ind. B 8, 588–595. https://doi.org/10.1016/ j.ngib.2021.11.006.
- Xiong, Y., Hou, Z.M., Tan, X.C., Luo, J.S., Yue, Y., Wu, K.Y., 2021. Constraining fluid-rock interactions during eogenetic karst and their impacts on carbonate reservoirs: insights from reactive transport modeling. Appl. Geochem. 131, 105050. https://doi.org/10.1016/j.apgeochem.2021.105050.
- Yadav, R., Naik, S.S., Naidu, P.D., 2021. Contrasts in calcium carbonate dissolution above the lysocline in the equatorial Indian Ocean over the last~ 40 ka. Mar. Geol., 106717 https://doi.org/10.1016/j.margeo.2021.106717.
- Zeng, L.B., Wang, H.J., Gong, L., Liu, B.M., 2016. Impacts of the tectonic stress field on natural gas migration and accumulation: a case study of the Kuqa Depression in the Tarim Basin, China. Mar. Petrol. Geol. 27 (7), 1616—1627. https://doi.org/10.1016/j.marpetgeo.2010.04.010.
- Zeng, L.B., Gong, L., Guan, C., Zhang, B.J., Wang, Q.Q., Zeng, Q., Lyu, W.Y., 2022. Natural fractures and their contribution to tight gas conglomerate reservoirs: a case study in the northwestern Sichuan Basin, China. J. Petrol. Sci. Eng. 210, 110028. https://doi.org/10.1016/j.petrol.2021.110028.
- Zeng, L.B., Gong, L., Zhang, Y.Z., Dong, S.Q., Lyu, W.Y., 2023. A review of the genesis, evolution, and prediction of natural fractures in deep tight sandstones of China. AAPG Bull. 107 (10), 1687–1721. https://doi:10.1306/07052322120.
- Zhang, H., Cai, Z.X., Hao, F., Qi, L.X., Yun, L., Jiang, L., 2018. Hydrogeomorphologic architecture of epikarst reservoirs in the middle-lower ordovician, Tazhong uplift, Tarim Basin, China. Mar. Petrol. Geol. 98, 146–161. https://doi.org/ 10.1016/j.marpetgeo.2018.08.008.
- Zhang, S., Jin, Q., Hu, M.Y., Han, Q.C., Sun, J.F., Cheng, F.Q., Zhang, X.D., 2021. Differential structure of Ordovician karst zone and hydrocarbon enrichment in paleogeomorphic units in Tahe area, Tarim Basin, NW China. Petrol. Explor. Dev. 48 (5) 1113–1125 https://doi.org/10.1016/S1876-3804/21360095-2
- 48 (5), 1113–1125. https://doi.org/10.1016/S1876-3804(21)60095-2. Zhong, J.H., Mao, C., Li, Y., Li, Y., Yuan, X.C., Niu, Y.B., Chen, X., Huang, Z.J., Shao, Z.F., Wang, P.J., Li, J., Zhang, D.F., 2012. Discovery of the ancient ordovician oilbearing karst cave in Liuhuanggou, North Tarim basin, and its significance. Sci. China Earth Sci. 55 (9), 1406–1426. https://doi.org/10.1007/s11430-012-4467-3.
- Zhong, J.H., Li, Y., Yuan, X.C., Mao, C., Niu, Y.B., Wei, H.H., Gao, J.B., Ni, L.T., Sun, N.L., Xue, C.Q., Dou, S.L., Liu, Y.X., Ren, K.X., Sheng, P.P., Wang, Y.H., Zhang, J.Z., Mu, G.H., 2021. A new structure-cave system: fold-cave composite. China J. Geol. 56 (4), 1001–1014. https://doi.org/10.12017/dzkx.2021.052.